Nearby Supernova Rates from the Lick Observatory Supernova Search. I. The Methods and Database

Jesse Leaman[1,2]⋆, Weidong Li[1]⋆, Ryan Chornock[1,3]⋆, and Alexei V. Filippenko[1]⋆

[1]*Department of Astronomy, University of California, Berkeley, CA 94720-3411, USA*
[2]*NASA Ames Research Center, Mountain View, CA 94043, USA*
[3]*Harvard-Smithsonian Center for Astrophysics, 60 Garden Street, Cambridge, MA 02138, USA*

8 December 2010

ABSTRACT

This is the first paper of a series in which we present new measurements of the observed rates of supernovae (SNe) in the local Universe, determined from the Lick Observatory Supernova Search (LOSS). We have obtained 2.3 million observations of 14,882 sample galaxies over an interval of 11 years (March 1998 through Dec. 2008). We considered 1036 SNe detected in our sample and used an optimal subsample of 726 SNe (274 SNe Ia, 116 SNe Ibc, 324 SNe II) to determine our SN rates. This is the largest and most homogeneous set of nearby SNe ever assembled for this purpose, and ours is the first local SN rate analysis based on CCD imaging and modern image-subtraction techniques. In this paper, we lay the foundation of the study. We derive the recipe for the control-time calculation for SNe with a known luminosity function, and provide details on the construction of the galaxy and SN samples used in the calculations. Compared with a complete volume-limited galaxy sample, our sample has a deficit of low-luminosity galaxies but still provides enough statistics for a reliable rate calculation. There is a strong Malmquist bias, so the average size (luminosity or mass) of the galaxies increases monotonically with distance, and this trend is used to showcase a correlation between SN rates and galaxy sizes. Very few core-collapse SNe are found in early-type galaxies, providing strong constraints on the amount of recent star formation within these galaxies. The small average observation interval ($\sim$ 9 d) of our survey ensures that our control-time calculations can tolerate a reasonable amount of uncertainty in the luminosity functions of SNe. We perform Monte Carlo simulations to determine the limiting magnitude of each image and the SN detection efficiency as a function of galaxy Hubble type. The limiting magnitude and the detection efficiency, together with the luminosity function derived from a complete sample of very nearby SNe in Paper II, will be used to calculate the control time and the SN rates in Paper III.

Key words: surveys — supernovae: general — supernovae: rates — galaxies: evolution

1 INTRODUCTION

Supernovae (SNe), which occur in several spectroscopically distinct varieties (e.g., Wheeler & Harkness 1990; Filippenko 1997), represent the final, explosive stage in the evolution of certain varieties of stars, and are among the most interesting and important constituents of the Universe. SNe provide a celestial laboratory to study stellar evolution. They synthesise and expel heavy elements, thereby dictating much of the chemical evolution of galaxies. Shock waves from SNe inject energy into the interstellar media of galaxies and may also trigger vigorous bursts of star formation. They lead to the formation of neutron stars, and probably even black holes under some circumstances. Some SNe are associated with energetic gamma-ray bursts. Being so powerful and calibratable in their observed properties, Type Ia supernovae (SNe Ia) are exceedingly useful cosmological probes; they led to the discovery of the accelerating expansion of the Universe (Riess et al. 1998; Perlmutter et al. 1999; see Filippenko 2005 for a review).

The rate of SNe is a key quantity for astrophysics. Measurements of the SN rate and its evolution over cosmic time

⋆ E-mail: jleaman@astro.berkeley.edu   (JL), wli@astro.berkeley.edu   (WL),   rchornock@cfa.harvard.edu (RC), alex@astro.berkeley.edu (AVF)

provide important information on the metal enrichment and chemical evolution of the Universe; the structure, kinematics, and composition of the interstellar medium; the birth rate of compact objects; and the formation of SNe from different types of progenitor systems.

Over the past seventy years, many studies have attempted to measure the SN rate in the local Universe and at moderate to high redshifts. There are both advantages and disadvantages of measuring the SN rate in nearby galaxies. The nearby SNe are bright and can be easily observed with small to moderate-sized telescopes. Information on the host galaxies such as the Hubble type, luminosity, and colour are more readily available for the nearby galaxies than for the more distant ones, making it possible to do detailed studies of the rate dependence on SN environment. On the other hand, nearby SNe are relatively rare, so it takes a long time to accumulate enough statistics. It is also difficult to do an all-sky survey for the nearby SNe; thus, most nearby searches have, in the past, conducted targeted snapshots of a sample of known galaxies. Determination of the SN rate from such targeted surveys requires the "control-time method" (see §3 and the Appendix), which historically has been plagued with uncertainties in the photometric behaviour of SNe, their luminosity function (LF), and the extinction they experience in their host galaxies. The monitoring of a predetermined galaxy sample also has the potential to introduce selection biases.

Van den Bergh (1991) summarises estimates of nearby SN rates before the 1990s. These earlier rates are based mostly on the Palomar SN search (Zwicky 1938, 1942), the Asiago SN search (Cappellaro & Turatto 1988), and Robert Evans' visual search (van den Bergh, McClure, & Evans 1987; van den Bergh & McClure 1990). The SN rate was first expressed as the frequency of SNe in an average galaxy, but it was realised that this frequency is proportional to the host-galaxy luminosity (Pskovskii 1961, 1967; however, see the discussion in Paper III for a nonlinear proportionality). Accordingly, the SN rate is generally normalised by the galaxy luminosity and given in units of SNu, or 1 SN $(100 \text{ yr } 10^{10} \text{ L}_\odot)^{-1}$.

In the past two decades, the most influential studies of nearby SN rates were conducted by Cappellaro et al. (1993a, 1993b, 1997, 1999). In particular, Cappellaro et al. (1999; C99, hereafter) combined five surveys to increase the total number of SN discoveries to 136.[1] The SN rates, normalised to the B-band luminosity of the host galaxies, were measured for galaxies of different Hubble types, and were compared to different tracers of star formation (e.g., broad-band colours, far-infrared luminosities).

The C99 database is the heart and soul of numerous studies of the SN rate. Mannucci et al. (2005; hereafter M05) normalised the rates with the infrared K-band luminosity, as well as with the mass derived from the K-band luminosity and $B - K$ colours of the galaxies. Della Valle et al. (2005) found that radio-loud early-type galaxies have a SN Ia rate that is a factor of 4 higher than that of the radio-quiet early-type galaxies, and suggested that the enhance-

ment is probably caused by repeated episodes of interaction and/or merger events. Mannucci et al. (2008) investigated the cluster early-type galaxy SN Ia rate, and found that it is more than three times larger than that in field early-type galaxies, perhaps due to galaxy interactions in the clusters. Mannucci et al. (2005, 2006) further derived delay-time distributions of SNe Ia, and postulated that there may be two components in the SN Ia population: a "prompt" component with the SNe Ia exploding soon after their stellar birth, and a "tardy" component with the SNe Ia exploding after a long delay following star formation. The implications of the two-component model on the progenitors of SNe Ia and the impact on their use as calibratable candles to derive cosmological parameters are further discussed by Scannapieco & Bildsten (2005), Sullivan et al. (2006), and Dahlen et al. (2008).

Because of the growing interest in using the evolution of the SN Ia rate over cosmic time to constrain the progenitor systems of SNe Ia, numerous recent studies have derived SN Ia rates at moderate to high redshifts (e.g., Hardin et al. 2000; Madgwick et al. 2003; Tonry et al. 2003; Blanc et al. 2004; Strolger et al. 2004; Dahlen et al. 2004, 2008; Neill et al. 2006; Poznanski et al. 2007; Botticella et al. 2008; Dilday et al. 2008; Horesh et al. 2008). Many of these investigations were conducted with systematic rolling searches using large ground-based telescopes or the *Hubble Space Telescope*, yielding rates that have precisions comparable or superior to those of the published nearby SN rates. Thus, it is critical to improve the precision of the nearby SN rates before they become the bottleneck for studies of the cosmic evolution of SN rates.

In this series of papers, we report the determination of nearby SN rates from our long-term efforts with the Lick Observatory Supernova Search (LOSS). LOSS, conducted with the 0.76-m Katzman Automatic Imaging Telescope (KAIT), has been described by Li et al. (2000), Filippenko et al. (2001), Filippenko (2003, 2005), and Filippenko, Li, & Treffers (2011). KAIT, based on the prototype Berkeley Automatic Imaging Telescope (Richmond, Treffers, & Filippenko 1993), is a fully robotic telescope whose control system checks the weather and performs observations with a dedicated CCD camera without human intervention. The data are automatically processed through an image-subtraction pipeline (Ganeshalingam et al. 2010; Filippenko et al. 2011), and candidate SNe are flagged. The next day, these candidates are visually inspected by a group of students (primarily undergraduate) in the Department of Astronomy at the University of California, Berkeley. The most promising SN candidates are reobserved the next clear night, and the confirmed SNe are reported to the Central Bureau of Astronomical Telegrams (CBAT). During the period from March 1998 through the end of 2008 (on which the data from this study are based), LOSS found 732 SNe, easily exceeding any other searches for nearby SNe and accounting for more than 40% of all SNe with redshift $z < 0.05$ reported to the Central Bureau for Astronomical Telegrams.

This is Paper I of a series of several papers, and is organised as follows. Section 2 provides an outline of the series, summarises the improvements of our rate determination over the published results, and discusses possible limitations of our study. In §3 we describe the control-time method for a family of light curves with a known LF. Section 4 discusses

---

[1] As noted by Mannucci et al. (2005), one of the 137 SNe used in C99 was later discovered to be associated with a galaxy not included in the sample.

the galaxy and SN samples, and other key ingredients in the rate calculations, including the log files, the limiting-magnitude determination, and the detection efficiency. Our conclusions are summarised in §5. Throughout the study, we adopt the WMAP5 Hubble constant of $H_0 = 73$ km s^{-1} Mpc^{-1} (Spergel et al. 2007), consistent with the recent direct determination based on Cepheid variables and SNe Ia by Riess et al. (2009).

2 SERIES OUTLINE AND SUMMARY OF IMPROVEMENTS

2.1 Outline of the Series

Paper I (this paper) lays the foundation for our study. It discusses the control-time method for SNe with a known LF, and provides detailed information on the galaxy and SN samples. The physical parameters (Hubble type, colours, mass, inclination, etc.) of the LOSS sample galaxies are studied to check whether they are typical of the normal volume-limited galaxy distribution. The various subsamples of galaxies and SNe are also described. The paper then discusses the log files used in the rate calculations, and shows some statistics on the observation-interval distribution in our search. We also report how the limiting magnitudes are derived for each KAIT image based on several parameters in the log files. Finally, we use Monte Carlo simulations to study the detection efficiency — that is, how our image-processing software handles detections of SNe with different significance. The limiting magnitude and the detection efficiency are key ingredients in the control-time calculations.

Paper II (Li et al. 2011a) reports the determination of the observed LFs of SNe, an important piece of information for the control-time calculation. This is the first time such LFs have been derived; they eliminate uncertainties in the historical SN rate calculations caused by uncertainties in the assumed SN light curves, the peak-magnitude distribution, and the host-galaxy extinction. We first constructed a distance-limited sample of 175 SNe ($D < 60$ Mpc for the core-collapse SNe Ibc and II, $D < 80$ Mpc for the SNe Ia), and then measured the light curve for every SN from either the SN search images or the dedicated follow-up photometry. A family of light curves was then used to fit the peak observed magnitude of each SN, and the observed absolute magnitude of the SN was calculated. For each SN, the completeness of our survey is determined from the monitoring history. We study the dependence of the SN LF on the host galaxy and SN subtype properties, and report the observed fraction of different subtypes of SNe and LFs in a magnitude-limited survey.

Paper III (Li et al. 2011b) uses all of the information presented in the first two papers and calculates the control time for the KAIT sample galaxies. We show that our SN rates have a significant correlation with the distance bin used for the calculation, and demonstrate that this is caused by a "rate-size relation": the SN rates, after being normalised linearly by the size (luminosity or mass) of their host galaxies, are still correlated with the galaxy size, in the sense that smaller galaxies have higher rates. A rate-size slope (RSS, hereafter) is used to normalise the rates to the same galaxy size. The RSSs for different normalisations are estimated

and are used to derive the rates. The SN rates for different types of SNe are reported for galaxies of different Hubble types and colours. We compare our rates to the published C99/M05 results and find that our rates, with more bins and smaller error bars, are in good agreement with the published measurements when the rates are calculated in the same manner. We also derive the expected SN rate in the Milky Way Galaxy and the volumetric rates in the local Universe. Discussions of the possible causes of the rate-size relation, and of the two-component model fit for SN Ia rates, are also provided.

Using a subset of LOSS sample galaxies having Sloan Digital Sky Survey (SDSS) spectra, Paper IV (Maoz et al. 2011) developed a robust method to recover the SN delay time distribution (DTD) — the SN rate versus time that would follow a brief burst of star formation — and found strong evidence for populations of SNe Ia in both "prompt" (age < 420 Myr) and "delayed" (age > 2.4 Gyr) stellar populations.

2.2 Summary of Improvements over Published Results

Our study improves upon previously published results in a number of ways, as follows.

(1) *Increased sample size.* Small-number statistics have been a key issue in calculations of nearby SN rates. The C99 study had to combine five different surveys (one conducted visually and four done with photographic plates) to increase the number of SN discoveries to 136, but at the expense of introducing heterogeneity. Our study considered 1036 SNe detected in the KAIT fields, and used an optimal subset of 726 SNe in the final rate calculation. This is more than five times the number of SNe used by C99.

(2) *Fewer observational biases.* The benchmark work of C99 inherited uncertain biases associated with the limited dynamic range of human vision and photographic plates. Our rate calculation, on the other hand, is based on a single systematic CCD survey with a modern image-subtraction processing pipeline. Consequently, we are able to more fully investigate potential observational biases involved in the rate calculations. In particular, our final rates are based on an optimal subsample of SNe that excludes the SNe that occurred in early-type galaxies of small radius (to avoid the uncertainty in the detection efficiency) and in highly inclined late-type galaxies (to avoid the uncertain correction factor for galaxy inclination).

(3) *Improved quality of the SN sample.* Of the 726 SNe in the optimal sample, only 12 ($< 2\%$) do not have a spectroscopic classification. For many of the SNe, we have our own optical spectra. There are also subclass types for a significant number of SNe, especially in the complete sample of very nearby SNe (Paper II), enabling us to provide information on the relative fractions of different subtypes of SNe.

(4) *Fewer uncertainties in the control-time calculation.* The observed LF in Paper II enables us to avoid several uncertainties that have historically plagued SN rate determinations, namely the peak-magnitude distribution and the host-galaxy extinction. In fact, our derived LFs should help with all future SN rate calculations.

(5) *Improved rate-calculation method.* We identify a

trend between the normalised SN rates and the sizes of the galaxies, and are able to evaluate the rates in a nominal galaxy size. The rate for a galaxy of any given size is evaluated with a rate-size relation.

2.3   Possible Limitations of Our SN Rates

There are considerable differences between the LOSS sample galaxy properties and those from a complete, volume-limited galaxy sample. As detailed in §4, the LOSS galaxy sample has a significant deficit in faint[2] galaxies, especially in the more-distant bins. This could lead to the belief that our SN rates are only applicable to luminous galaxies. However, there are three reasons we think our rates can be applied to the general population of galaxies, as follows.

(1) Even though the LOSS galaxy sample is not complete at the low-luminosity end, there is a sufficient number of low-luminosity galaxies to provide a reliable rate calculation. In fact, the SN rate in faint galaxies is the cornerstone for the rate-size relation that we discovered.

(2) From our studies of the SN LFs in Paper II, no significant differences in the LFs are found for galaxies having different sizes, with a possible exception for SNe II in late-type spiral galaxies. Even in the late-type spiral galaxies, the differences in the LFs are probably caused by a change in the composition of different SN subtypes rather than in the luminosities for a particular SN subtype.

Nevertheless, the possible change of composition for the subtypes of SNe II in late-type spiral galaxies, and the growing evidence that certain kinds of SNe are preferentially found in extremely low-luminosity, low-metallicity galaxies (e.g., Modjaz et al. 2008; Miller et al. 2009; Drake et al. 2009; Quimby et al. 2009), lead us to encourage caution when using our rates in very low-luminosity galaxies. In the same vein, the reported observed fractions of different SN subtypes (Paper II) should be used with caution for the very low-luminosity galaxies. Recently, Arcavi et al. (2010) reported a complementary study of a sample of 70 core-collapse SNe found by the Palomar Transient Factory (PTF), an untargeted survey that monitors many low-luminosity galaxies; see §5.4 of Paper II for more details.

3   THE CONTROL-TIME METHOD FOR SUPERNOVAE WITH A KNOWN LUMINOSITY FUNCTION

The "control time" is defined as the total interval of time during which a SN, of a given type and photometric evolution, would have been bright enough to have been discovered during all of the observations of a given galaxy. The use of the control time to calculate the SN rate was first introduced by Zwicky (1942) and refined by van den Bergh (1991) and Cappellaro et al. (1993a, 1997). The idea of being able to "control" a galaxy stems from the fact that SNe are transient phenomena, and only stay visible for a certain length of time.

The mathematical details of the control-time method

used in our rate calculations are discussed in the Appendix. We have generalised the basic control-time method to the case of a SN type for which we know the LF. In our study, the LFs are composed of discrete components corresponding to individual peak magnitudes *and light-curve shapes* of SNe found in a distance-limited sample, as determined in Paper II. Our definition of the LF is thus slightly different from the conventional case where the luminosity function is defined as the number of sources per unit luminosity interval.

In particular, Equation (A11) is the foundation of our control-time calculations, and is reproduced here:

$$t = \sum_{i=1}^{n} f_i t_i, \tag{1}$$

where t is the total control time, t_i is the control time from the i-th component in the LF, and f_i is the fraction of the LF due to the i-th component. This equation indicates that the total control time for a given type of SN with a known LF is the sum of the control times of each component weighted by the fractional contribution of that component to the LF.

4   THE DATABASE

4.1   The Galaxy Sample

4.1.1   The Construction of the Galaxy Sample

The LOSS sample galaxies were selected mainly from the Third Reference Catalog of Bright Galaxies (RC3; de Vaucouleurs et al. 1991). A detailed description of the selection process is presented elsewhere (Filippenko et al. 2011). For the period between March 1998 and the end of 1999, a small sample of ~ 6000 fields was used. The sample was expanded to about 15,000 fields during the year 2000, and this is the galaxy sample that will be discussed here. We also note that the sample was enlarged to roughly 20,000 fields during the nearly three-year period between Oct. 2000 and July 2003 when LOSS was temporarily expanded to LOTOSS (the Lick Observatory and Tenagra Observatory SN search; Schwartz et al. 2000).

Although the KAIT camera has a relatively small field of view ($6.7' \times 6.7'$), there are multiple galaxies in some of the fields. It is thus important to have a set of criteria to define which galaxies are monitored during our SN search. As our goal is to conduct detailed studies of the SN rates in different environments, we require a galaxy to have the following information to be included in the galaxy sample: the redshift or distance, the Hubble type, and the luminosity in at least one of the B or K bands. We also limit our sample galaxies to $z < 0.05$ (recession velocities smaller than 15,000 km s^{-1}).

To collect information on the KAIT sample galaxies, we have used exclusively two large online astronomical databases: the NASA/IPAC Extragalactic Database (NED)[3] and HyperLeda (Paturel et al. 2003)[4]. We first searched all of the galaxies in the KAIT fields in NED, and found 76,355 objects. The coordinates for these galaxies were then sent to HyperLeda to collect additional information.

---

[2] Hereafter, "faint" refers to low intrinsic luminosity unless otherwise specified.

[3] http://nedwww.ipac.caltech.edu
[4] http://leda.univ-lyon1.fr

The requirement of having a recession velocity smaller than 15,000 km s^{-1} cut the sample to 21,190 galaxies; most of the excluded galaxies do not have redshift information, are visually faint, and are in the background of the primary KAIT galaxies. We used the recession velocities corrected for the infall of the Local Group toward the Virgo Cluster ("vvir" in HyperLeda), and we adopted $H_0 = 73$ km s^{-1} Mpc^{-1} to calculate the distance. For a few very nearby galaxies with negative recession velocities, we were able to find distance estimates using the VizieR service (Ochsenbein et al. 2000)[5].

We group the Hubble types of the galaxies into eight bins (Table 1). These bins can also be grossly labeled as early-type galaxies (No. 1 to 2), early-type spiral galaxies (No. 3 to 5), and late-type spiral or irregular galaxies (No. 6 to 8). Although on average the classifications from NED and HyperLeda are consistent with each other (the difference, using the numbering scheme in Table 1, is 0.15±0.69 for 11,754 galaxies that have classifications in both databases), there is a tendency for HyperLeda to put galaxies having an Scd classification in NED into the Sc category. Consequently, the statistics in the Scd galaxy bin become rather poor. We find that the NED classifications are more consistent with those published in RC3, from which most of our sample galaxies are selected; thus, we have adopted the Hubble types from the NED database.

Note that the Hubble-type information in NED comes from many different sources and is therefore quite inhomogeneous. In fact, there are ~ 2600 Hubble-type designations in the database, and we had to construct a conversion table to put them into our 8 well-defined bins. We also note that Sydney van den Bergh, together with our group, has classified the LOSS SN host galaxies in the DDO morphological type system (van den Bergh, Li, & Filippenko 2002, 2003, 2005). However, to perform SN rate calculations using this very homogeneous classification scheme, we would also need DDO classifications for all of the KAIT sample galaxies not having a SN discovery, and we were unable to do this.

For the photometry of the galaxies, we used "btc" from HyperLeda for the B band and "k_m_ext" from the 2MASS catalog for the K band. Here, "btc" is the apparent total B magnitude corrected for Galactic extinction, internal extinction due to the inclination of the host galaxy, and the K-correction. The Galactic extinction is adopted from Schlegel, Finkbeiner, & Davis (1998). The internal extinction is computed following Bottinelli et al. (1995), and is a function of the Hubble type and the axial ratio. The K-correction is calculated from a simple recipe given by de Vaucouleurs et al. (1976), and is a function of the host-galaxy Hubble type and recession velocity. The value "k_m_ext" is the total K-band photometry obtained by extrapolating the fit of a Sersic function to the radial profile, and is best suited for extended objects such as galaxies (see Jarrett et al. 2003, for details).

To calculate the inclinations of the galaxies, which are important for the investigation of the inclination correction factor for the SN rate, we follow the traditional Hubble (1926) formula

$$\text{Incl} = \begin{cases} 90° & \text{if ratio} \leqslant 0.20, \\ \text{acos}\left(\sqrt{\frac{\text{ratio}^2 - 0.20^2}{1.0 - 0.20^2}}\right) & \text{otherwise,} \end{cases} \qquad (2)$$

where "ratio" is the ratio of the apparent minor and major axes of the galaxy. This simple formula works well for most of the spiral galaxies, but perhaps not for the irregular and early-type galaxies (van den Bergh 1988).

The requirement to have the Hubble type and photometry results in further cuts to our galaxy sample, and our final sample has 14,882 galaxies (hereafter, the "full" galaxy sample). All of the galaxies in this sample have Hubble-type information, 98.6% have B-band photometry, and 91.8% have K-band photometry. The first 20 entries of this galaxy sample are shown in Table 2, and the rest of the entries are available electronically. The meaning of the different columns in Table 2 is as follows: (1) the internal name for the field, (2) the name of the galaxy, (3) the right ascension (α) in degrees, (4) the declination (δ) in degrees, (5) the distance in Mpc, (6) the source of the distance, (7) the Hubble type in numerical code as listed in Table 1, (8) the source of the Hubble type, (9) the diameter of the major axis in arcmin (isophotal level of 25 mag arcsec^{-2} in the B band), (10) the diameter of the minor axis in arcmin, (11) the inclination in degrees, (12) the source of Cols. 9–11, (13) the position angle, (14) the Galactic reddening, (15) the internal extinction due to galaxy inclination, (16) the total apparent B magnitude, (17) the uncertainty in Col. 16, (18) the corrected total apparent B magnitude "btc," (19) the K magnitude from 2MASS, and (20) the uncertainty in Col. 19.

Four subsamples of galaxies are used throughout our study. The "full" sample has all 14,882 galaxies as discussed above. The second subsample excludes all of the small early-type galaxies (with major axis $< 1.0'$; see details in §4.5), and is called the "nosmall" sample. The third subsample excludes all of the small early-type galaxies and the highly inclined spiral galaxies (incl. $> 75°$), and is the galaxy sample for the optimal subset of SNe used for the rate calculations (hereafter, the "optimal" galaxy sample). The fourth subsample includes all of the galaxies within 60 Mpc in the "nosmall" galaxy sample, and is the galaxy sample for the core-collapse (hereafter, CC) SNe considered in the LF study in Paper II (hereafter, the "LF-CC" galaxy sample). The information on all of these subsamples is available electronically.

A key question about the LOSS sample galaxies is whether they are representative of the general population. In the following sections, we compare the LOSS galaxy LF to the published results from a complete galaxy sample, and provide statistics on the physical parameters of the LOSS sample galaxies and their evolution with distance.

4.1.2 The LOSS Galaxy Luminosity Function

The upper panel of Figure 1 plots the LOSS galaxy LF for the "full" sample. To calculate the absolute K-band magnitudes, the K-band magnitudes in Table 2 are corrected for Galactic extinction following the Galactic reddening law with $R_V = 3.1$ by Cardelli, Clayton, & Mathis (1989). No internal extinction due to galaxy inclination is considered, but it is likely to be minimal. The solid curve is for all of the galaxies with a K-band measurement (13,635 galaxies), while the dashed line is for 5008 galaxies within 60 Mpc

(i.e., the LF-CC galaxy sample). The LFs are shifted arbitrarily to facilitate comparison. Also plotted (the smooth solid curve) is the K-band luminosity function for a complete galaxy sample by Kochanek et al. (2001; the Kochanek curve, hereafter) derived from a sample of 4192 galaxies in the 2MASS survey[6], shifted to visually fit the bright end of the LF-CC sample. The dash-dotted line marks $L_K = 7 \times 10^{10}$ L$_\odot$ (or $M(K) = -23.7$ mag), which is the nominal galaxy size used in Paper III.

Compared to the complete sample, there is a clear deficit of low-luminosity galaxies in the LOSS samples. The LF for the "full" sample is dramatically different from the Kochanek curve: the rise at the luminous end is not as steep, and there is a clear downturn for galaxies fainter than $M(K) = -24.5$ mag. However, there is also a considerable number of low-luminosity galaxies in the LOSS sample: 50% of the galaxies in the "full" sample are fainter than $M(K) = -23.7$ mag (the nominal galaxy luminosity, about the size of the Milky Way). 1236 galaxies (8% of the total) are fainter than $L_K = 0.7 \times 10^{10}$ L$_\odot$, 10% of the size of the nominal galaxy size adopted in Paper III. Within these low-luminosity galaxies, 26 SNe were discovered and used in the rate calculations. As shown in Paper III, despite the incompleteness of the LOSS galaxies at the low-luminosity end, there are sufficiently high statistics in both the number of SNe discovered and the control time of the galaxies to allow a reliable rate calculation to be performed.

For the LF-CC sample of nearby galaxies (distance < 60 Mpc), although the deficit at the low-luminosity end is still clearly present, the bright end ($L_K > 7 \times 10^{10}$ L$_\odot$) can be well fit by the Kochanek curve. This likely means that for these nearby galaxies, the LOSS galaxy sample is representative of the complete galaxy sample at the bright end. This is important, because even though the LF-CC sample misses a significant fraction of galaxies at the low-luminosity end (compared to the Kochanek curve) in terms of numbers, the missing fraction is not significant in terms of luminosity (and thus in the number of SNe). This is demonstrated in the lower panel of Figure 1. Here the luminosity is plotted on the abscissa using a linear scale, while the ordinate shows the number of the galaxies multiplied by the luminosity and the CC SN rate[7] in Paper III. Effectively, this plot illustrates the contribution to the total number of CC SNe from each luminosity bin. The contribution peaks at the nominal galaxy size, has a long tail at the bright end of the galaxies, and a sharp decline at the faint end. The curve for the complete sample (the solid smooth curve) is also plotted, and is visually scaled to fit the bright end of the LF-CC sample. Even though the contribution to the total CC SNe peaks at a smaller luminosity ($L_K \approx 4 \times 10^{10}$ L$_\odot$) for the complete galaxy sample, the difference in the total number of SNe (the integrals of the two curves) suggests that the LF-CC sample misses about 15% of the CC SNe due to the deficit in the low-luminosity galaxies relative to the complete galaxy

sample.[8] A similar analysis is performed for the SNe Ia, and only $\sim 10\%$ are missed.

We note that these small fractions of missed SNe (compared to the complete galaxy sample) are consistent with the expectations from a study by Brinchmann et al. (2004), who suggested that the majority of the star formation in the local Universe takes place in moderately massive galaxies, typically in high surface brightness disk galaxies. The low-luminosity galaxies, though numerous, do not add much to the total star formation (or total luminosity) and hence do not produce many SNe. These results have important implications in Paper II, where we use the SNe discovered in the very nearby galaxies to construct a complete, volume-limited SN sample.

Although the LF-CC sample is representative of the complete galaxy sample at the luminous end, the sample is not complete to all galaxies within 60 Mpc. First, as detailed by Filippenko et al. (2011), our survey is limited to declinations between $-25°$ and $+70°$ due to the physical limitation of KAIT, which means we can only access $\sim 70\%$ of the all-sky volume. Since we obtained snapshot images of a sample of galaxies, the extensive regions in between the galaxies are not monitored either. We can estimate the degree of completeness for our galaxy sample by comparing the total luminosity to the expectation from the published local luminosity density. The total L_K in the LF-CC sample is 1.5×10^{14} L$_\odot$. Using the local luminosity density as adopted in Paper III (from Kochanek et al. 2001), the all-sky total luminosity for the galaxies within 60 Mpc is $L_K = 4.7 \times 10^{14}$ L$_\odot$. This means that our sample galaxies account for $\sim 45\%$ of the total stellar light accessible by our survey.

4.1.3   The Properties of the LOSS Sample Galaxies

Figure 2 shows some properties of the LOSS sample galaxies. The upper-left panel illustrates the distribution of Hubble types. The open histogram is for the "full" galaxy sample, while the shaded region is for the nearby LF-CC sample. Unfortunately, we could not find a study of the expected Hubble-type distribution for a complete galaxy sample, but it seems that the "full" galaxy sample has plenty of galaxies in each Hubble-type bin except the irregular galaxies. This deficit is most likely caused by the incomplete information for these visually faint, extended objects in the current astronomical databases. In fact, because of the relative lack of "Irr" galaxies in the sample, there are just a few SNe discovered in this galaxy bin, resulting in only an upper limit for many rate calculations. This is currently being remedied in our search, as we recently started to monitor additional LOSS fields centered on known irregular galaxies. The LF-CC sample (the shaded histogram) has an increasingly larger fraction of the "full" sample from E to Irr galaxies. As discussed in §4.1.4, this is not surprising, as more galaxies of lower surface brightness are missing from the LOSS sample in more-distant bins.

---

[6] This sample of galaxies is magnitude limited, but is corrected to be volume limited (complete) based on the survey volume of each limiting magnitude; see Kochanek et al. (2001) for details.

[7] The rate used here is derived from SNe in all of the Hubble types. Also, the rate-size relation in the K band as derived in Paper III is employed.

[8] We note that this does not mean that our CC SN rate is off by 15%, since the rate will be recovered when the control time is considered.

The upper-right panel shows the distribution of the inclination angle for the "full" sample. In theory, there should be random lines of sight for the galaxies, so the distribution for the inclinations in degrees should follow a sine curve, but there is in fact a dearth of galaxies having very small inclinations (i.e., face-on galaxies). The reason for this is the limitation of the catalogued precision for the major and minor axes (typically $0.1'$). Most of the LOSS galaxies have a major axis (MaA, hereafter) smaller than $2'$, and require a precision better than $0.1'$ to yield an inclination smaller than $20°$. On the other hand, poor precision can also make a slightly inclined galaxy appear face-on, hence the weak peak at $0°$ in Figure 2.

The uncertainties in the inclination measurements have some impact on the results in our study. First, an error in the inclination would cause an error in the internal extinction calculation to the total B-band magnitude, and this in turn would affect the $B - K$ colour and the mass estimate for the galaxy. Fortunately, for galaxies with inclinations below $20°$, the internal extinction is small (< 0.03 mag). Second, the inclinations are also used to study the inclination correction factors in the SN rates. For these reasons, we have grouped the inclinations into three broad bins: the "face-on" sample includes all galaxies with inclination smaller than $40°$, the "edge-on" sample is for inclinations larger than $75°$, and the "normal inclination" sample includes all of the rest. The broad bins are necessary because we want to include a reasonable number of galaxies in the "face-on" bin. Note that edge-on spiral galaxies are not included in the "optimal" galaxy sample.

The lower two panels in Figure 2 show the distribution of MaA in both arcmin and kpc for the "full" galaxy sample. The majority of the galaxies have MaA between $1'$ and $2'$. The median physical size of the galaxies is ~ 25 kpc.

One main result of our rate calculations in Paper III is that the normalised SN rate has a correlation with the size of the galaxies. We thus plot the average B and K luminosity and the mass of the galaxies in the "optimal" sample in Figure 3, and report their values (together with those for the "full" sample) in Table 3. The masses of the galaxies are calculated according to the prescription of M05 as a function of L_K and the $B - K$ colour: $\log(M/L_K) = 0.212(B - K) - 0.959$. Preliminary analysis (Dilday et al. 2011) of galaxy spectral energy distribution (SED) fits using PEGASE (Le Borgne et al. 2004) to multi-band SDSS photometry of a subset of our sample galaxies indicates that the masses determined using the method of M05 qualitatively agree well with those from the more detailed SED modeling, suggesting that the M05 prescription is reasonable. The top panel of Figure 3 shows the distribution in different Hubble types, while the bottom panel gives the distribution in different $B - K$ colours. It is clear that galaxies with different Hubble types or colours have different average sizes (a factor of 10 for the K-band luminosity and mass, and a factor of 2–5 for the B-band luminosity). Not surprisingly, the most massive galaxies are the red ellipticals.

4.1.4 The Evolution of LOSS Sample Galaxies with Distance

Although no cosmological evolution effect is expected for the nearby LOSS galaxies, we demonstrate in this section that there are important systematic changes in the galaxy properties due to selection biases over the 0 to ~ 200 Mpc distance range of our sample.

Figure 4 illustrates the distribution of several parameters as a function of distance. The upper-left panel shows the K-band luminosity of the "full" galaxy sample; each dot represents a galaxy. Also plotted is the average K luminosity in different distance bins. The dots show that at greater distances, low-luminosity galaxies tend to be missing. Consequently, the average K luminosity increases monotonically with increasing distance. This is due to a Malmquist bias; the current astronomical databases become increasingly incomplete for low-luminosity objects at greater distances. As discussed in Paper III (especially in its Appendix), the presence of this obvious Malmquist bias is the main reason for our discovery of a strong correlation between the SN rates and the sizes (luminosities or masses) of the host galaxies (i.e., the rate-size relation).

The lower-left panel shows the average K luminosity of galaxies in different distance bins, for two Hubble types (open circles for Scd, solid circles for E). The distribution of the E galaxies has been scaled to match the Scd distribution in the 0–50 Mpc range. It is evident that the Scd galaxies exhibit a more dramatic Malmquist bias than the E galaxies, due to their low surface brightness and the general absence of bright nuclei. The average K luminosity changes by a factor of 20 over the distance range 15 to 175 Mpc for the Scd galaxies, while the corresponding factor for the E galaxies is 4.

The upper-right panel displays the number of galaxies in different distance bins. From 0 to 60 Mpc, the number of galaxies per bin increases, as one would expect from a complete galaxy sample; the survey volume per bin progressively increases with distance. However, the distribution peaks at 60–70 Mpc, and then declines gradually at greater distances.

The lower-right panel shows significant differences in the number distribution with distance of two types of galaxies (solid line for E, dashed line for Scd). While the number of E galaxies per bin increases from 0 to 60 Mpc, stays nearly constant until 140 Mpc, and declines thereafter, the number of Scd galaxies per bin is almost constant from 0 to 80 Mpc and then declines sharply thereafter. Again, this reflects completeness differences in the current astronomical database for galaxies of different Hubble types. The low surface brightness Scd galaxies are only complete nearby, while the E galaxies are easier to observe and are complete to a greater distance.

Because galaxies of different Hubble types have different distributions with distance, the relative fractions of the Hubble types also change: there are more late-type spirals in the nearby distance bins, while the E galaxies dominate the most distant bins. The change in Hubble-type demography with distance has important implications for the SN rates and will be discussed throughout our study.

4.2 The SN sample

4.2.1 The Construction of the SN Sample

LOSS began in 1997 but found only a single SN of questionable nature during that year (SN 1997bs; Van Dyk et al. 2000). Numerous improvements were made during late

1997 and early 1998, including the replacement (in March 1998) of the original Photometrics CCD camera having a front-illuminated Thompson TH 7895 chip with an Apogee AP7 having a much more sensitive back-illuminated SITe 512 chip. For our SN rate calculations hereafter, we consider only the period March 1998 through December 2008 (about 10 years and 9 months), unless explicitly expressed otherwise.

To determine accurate SN rates, we need to consider not only the SNe found by LOSS itself, but also the ones first discovered by other groups which were subsequently found independently as part of our search. Although we keep log files of the SNe discovered in the LOSS fields, to ensure completeness, we cross-correlated the official list of all the discovered SNe on the CBAT website[9] with the LOSS fields, and generated a list of 1232 SNe that were within the field of view of these fields. After setting aside the 732 SNe first discovered by LOSS, we then went through the monitoring history of the fields of the other 500 SNe, checked the image-processing log files and the candidate reports, examined the reobservation history, and identified 304 SNe that were found independently during our search. Thus, LOSS discovered a total of 1036 SNe.

Of the 196 SNe that were missed by LOSS, (a) the vast majority were discovered by other searches at a time when KAIT was not actively monitoring their host galaxies (fields that are too far toward the west at the beginning of the night, or too far toward the east at the end of the night); (b) some are background SNe at higher redshifts in the fields of the targeted LOSS galaxies; and (c) three were very close to the nuclei of their host galaxies (SN 2002bs, Wei et al. 2002; SN 2004cm, Connolly 2004; SN 2006gy, Quimby 2006) and not detected by the LOSS image-processing software (see additional discussion in §4.5). None of the objects detected by the pipeline was overlooked due to human error (see §4.3).

We cross-correlated the 1036 SNe that were found directly or independently by LOSS with the "full" galaxy sample and selected 934 SNe for use in the rate calculations. Of the remaining 102 SNe that are within the LOSS fields but not considered in the rate calculations, 47 are in background galaxies (discussed further in Paper II), 19 have no or incomplete Hubble-type information for their host galaxies, and 36 have no known host-galaxy redshift or $z > 0.05$.

Our final total SN sample consists of 929 SNe, after five additional SNe were removed as follows. SN 2003dl (Graham & Li 2003) was reported as a LOSS discovery, but a careful reanalysis of the monitoring images using better template images than were available at the time of discovery suggest that there is no SN at the position of SN 2003dl; instead, the detection was likely caused by a random background fluctuation combined with an inferior template image. SN 2005md (Li 2005) was also discovered by LOSS. Modjaz et al. (2005) obtained a spectrum, and suggested the object to be similar to the SN IIb 1993J at early times based on its featureless, blue continuum. However, the SN nature of SN 2005md is now highly questionable, given that it rebrightened in 2008 (Li et al. 2008). SN 2005ha (Prasad et al. 2005) was discovered by LOSS in the nearby S0/a galaxy UGC 3457 ($D = 36$ Mpc). It was quite subluminous at peak brightness (-14.8

mag) and had a fast photometric evolution. A spectrum obtained by Hamuy, Maza, & Folatelli (2005) is inconclusive, showing only a hint of the Ca II near-infrared triplet in emission. It is possible that SN 2005ha belongs to the growing subclass of subluminous "Ca-rich SNe Ibc" (Filippenko et al. 2003; Perets et al. 2010). We will provide more analysis of SNe 2005md and 2005ha in a future paper, but for now they are not considered in the rate calculation. SNe 2002bj and 2004cs are also transients of uncertain identity, as discussed below, and were removed from the sample.

One of the great assets of our SN sample is the completeness of the spectroscopic classification: useful spectra were obtained of 917 out of the 929 SNe (98.7%), thanks to the dedicated efforts of several groups. In particular, the majority of the classifications were made with the Mt. Hopkins 1.5 m telescope by the SN group led by R. P. Kirshner at the Harvard-Smithsonian Center for Astrophysics. Many of the classifications were also made with the Lick Observatory 3 m Shane reflector by our own SN group (led by A.V.F.) at University of California, Berkeley. We compiled the spectroscopic classifications from several sources and checked for differences: (a) the official list of SNe on the CBAT website as mentioned above, which contains the classifications; (b) the Asiago SN catalog[10]; (c) the SN list maintained by M. W. Richmond[11]; and (d) a list of SNe and their classifications compiled by us over the years. When there were discrepant classifications, we consulted the original IAU Circulars and our spectroscopic database. In the end, we have self-consistent classifications for all of the spectroscopically observed SNe in the sample; we believe there is only a low level ($\sim 2\%$) of misclassifications.

In Paper II, we fit the light curves of the SNe in the LF sample, thus providing a consistency check for the spectral classifications. This process led to the following four revisions or removals.

(i) Filippenko & Chornock (2002) classified SN 2002au as a probable (but not definite) SN Ia. The light-curve fit in Paper II suggests that the object is instead a SN IIb. We analysed the spectrum observed by Filippenko & Chornock using the Supernova Identification code (SNID; Blondin & Tonry 2007), and indeed the best three spectral matches are all SNe IIb near maximum brightness.

(ii) Serduke et al. (2006) classified SN 2006P as a probable SN Ia at about 2 weeks past maximum brightness. The analysis of the light curve in Paper II instead suggests a SN Ibc classification. We again used SNID to analyse the spectrum, and the best three matches are all SNe Ic near maximum brightness.

(iii) SN 2002bj was classified as a SN II or IIn by Kinugasa et al. (2002). Reduction of our follow-up photometry reveals a peculiar light curve: the SN declined by ~ 5 mag over a short period of 15 d, faster than any other known SN (Poznanski et al. 2010). The two spectra we obtained of SN 2002bj do not exhibit obvious H Balmer lines, and show some resemblance to the peculiar SN Ibc 2006jc (Foley et al. 2007; Pastorello et al. 2007). On the other hand, Poznanski et al. (2010) argue that SN 2002bj may have been a ".Ia" supernova (Bildsten et al. 2007), or at least some

kind of strange partial explosion of a white dwarf. Given its uncertain classification, we have removed SN 2002bj from our present analysis and will consider it further in a future paper.

(iv) SN 2004cs (Li, Singer, & Boles 2004) does not have a spectroscopic classification published in the IAU Circulars, but Rajala, Fox, & Gal-Yam (2004) suggested that the object was a SN Ia based on its observed colours and the colour-typing method developed by Poznanski et al. (2002), Gal-Yam et al. (2004), and Poznanski, Maoz, & Gal-Yam (2007). We have an excellent unfiltered light curve of SN 2004cs which reveals rapid evolution not compatible with that of any observed SNe Ia. Analysis of a spectrum (A. Gal-Yam 2009, private communication; also illustrated by Rajala et al. 2005) indicates that SN 2004cs is similar to SN 2007J, which may have been a peculiar SN Ibc (Filippenko et al. 2007) or perhaps related to a certain odd subclass of SNe Ia (Foley et al. 2009). As with SN 2002bj, we have removed SN 2004cs from our present analysis and will consider it further in a future paper.

SNe are spectroscopically classified into three main categories: Ia, Ibc[12], and II, with subclasses in each category (for a review, see Filippenko 1997). While we concentrate our rate calculations on the three main classes, we also pay attention to the subclasses, especially for the SNe in the LF sample (see Paper II for details). SNe Ia are grouped into the following subclasses: (a) normal objects (e.g., Branch & Tammann 1992), (b) high expansion velocity objects (Benetti et al. 2005; Wang et al. 2009), (c) SN 1991T-like objects (Filippenko et al. 1992a; Phillips et al. 1992), (d) SN 1991bg-like objects (Filippenko et al. 1992b; Leibundgut et al. 1993), and (e) SN 2002cx-like objects (Li et al. 2003; Jha et al. 2006). The SN Ia nature of SN 2002cx-like objects is currently being debated (Valenti et al. 2009 — but see Foley et al. 2009, 2010), and their rate will be further discussed in a future paper. SNe Ibc are classified into (a) SNe Ib, (b) SNe Ic, (c) peculiar SNe Ibc (hereafter, Ibc-pec), and (d) SNe Ib/c (SNe Ib or Ic with uncertain subtype classification). SNe II are classified into (a) SNe II-P ("plateau" in the light curve), (b) SNe II-L ("linear" magnitude brightness decline after the peak), (c) SNe IIb, and (d) SNe IIn. Note that the classifications of SNe II require both spectroscopic and photometric information, and are thus possible only for a subset of the SNe in our sample (the LF SNe in Paper II).

Information for the SN sample is listed in Table 4. Only the first 20 entries are shown, with the rest available electronically. Each SN entry lists the following: the SN name, its host-galaxy name, the date of discovery, the right ascension (α) in degrees, the declination (δ) in degrees, the offsets (in arcsec) from the host-galaxy nucleus, the magnitude at the time of discovery, the classification, the discoverer, and the membership in the various subsamples in our SN rate analysis (discussed below in §4.2.2). Among the 929 SNe in the total SN sample, 372 are SNe Ia (40.0%), 144 are SNe Ibc (15.5%), 399 are SNe II (42.9%), and 14 have no spectroscopic classification (1.5%). For the 726 SNe in the "optimal" sample used in the final SN rate calculations, 274 are SNe Ia (37.7%), 116 are SNe Ibc (16.0%), 324 are

SNe II (44.6%), and 12 have no spectroscopic classification (1.6%). For the rate calculations, SNe without a spectroscopic classification are split into fractions of SNe Ia, Ibc, and II according to the statistics of the SNe having spectroscopic classifications. These fractions are also different from the observed fractions in a complete sample of very nearby SNe as discussed in Paper II.

In the following sections, we describe several aspects of our SN sample in an attempt to quantify the characteristics of the sample.

4.2.2 The Different SN Subsamples

Our study uses a relatively large number of subsamples, seven total, in order to thoroughly explore various issues.[13] The "full" sample includes all 929 SNe discussed above. The "full-nosmall" subsample excludes the SNe in small early-type galaxies (MaA $< 1'$), and has 884 SNe. The "full-optimal" subsample excludes the SNe in small early-type and edge-on spiral galaxies, and has 726 SNe.

In an attempt to alleviate uncertainties in the control-time calculations due to uncertainties in the LFs and the host-galaxy extinction distribution, we consider a subsample of SNe that were only discovered "in season" — that is, the SNe exploded during (not prior to) the active monitoring period of the galaxies. We set a simple criterion for a SN to be considered "in season": there had to be a nondetection deeper than the SN discovery magnitude shortly before the discovery was made. In other words, a SN discovered in the first image of a galaxy after a long break when the galaxy was too close to the Sun was not counted as an "in-season SN." Accordingly, for this subsample the control time for each galaxy does not consider the first image after a long break. Note that because of our small observation intervals, this first image was often the only instance when the control time even needed to be calculated using the light-curve shape and limiting magnitude (§4.3); thus, we largely eliminated the control time from the calculation.

We went through the monitoring history of all 929 SNe and identified 656 "in-season" SNe, which we call the "season" subsample. The "season-nosmall" subsample excludes the SNe in small early-type galaxies and has 617 SNe. The "season-optimal" subsample excludes the SNe in small early-type and edge-on spiral galaxies; it contains 499 SNe.

After we constructed the observed LFs (Paper II) and used them in our SN rate calculations, the necessity of using the various season subsamples is diminished. Nevertheless, these subsamples offer us a chance to compare the rate measurements from different subsamples, as we have done in Paper III. Compared to the "full" samples, the "season" subsamples sacrifice some SNe and thus are more susceptible to small-number statistics, but provide better tolerance to the uncertainties in the LFs.

A subset of 175 SNe in the "season-nosmall" subsample (CC SNe within 60 Mpc, and SNe Ia within 80 Mpc), which we call the "LF" subsample, is used to construct the LFs in Paper II.

---

[12] Here we use "Ibc" to generically denote the Ib, Ic, and hybrid Ib/c objects whose specific Ib or Ic classification is uncertain.

[13] The list of SNe in each of the various subsamples is available electronically.

4.2.3   The Hubble-Type Distribution of the SN Host Galaxies

Figure 5 shows the Hubble-type distribution for the host galaxies of the "full" SN sample. There is a significant difference between the distribution of the SN Ia hosts and that of the CC SN hosts, as we have previously reported (van den Bergh et al. 2002, 2003, 2005). Kolmogorov-Smirnov (hereafter, K-S) tests suggest that there is only a 2.0×10^{-9} and 1.0×10^{-20} probability that the SN Ia hosts come from the same population as the SN Ibc and SN II hosts, respectively. Even when the early-type galaxies (E–S0) are not considered, the SN Ia hosts still have a significantly different distribution compared with that of the CC SNe; the probability that they come from the same population is less than 2%. On the other hand, the hosts of SNe Ibc and SNe II have quite similar distributions, coming from the same population with 94.9% probability.

These results are not surprising, given the different progenitor systems for the different SN types. SNe Ia are generally thought to come from the explosion of an accreting white dwarf in a binary system, so they are frequently found among old or intermediate-age populations of stars. Core-collapse SNe (Ibc and II), on the other hand, come from stars that are more massive than 8–10 $M_\odot$, so they arise predominantly from young, star-forming populations. When translating this correlation into the Hubble-type distributions, SNe Ia are often found in E, S0, and early-type spiral galaxies, while SNe Ibc and II occur mostly in spiral galaxies.

There is a small fraction (13 out of 536; 2.4%) of CC SNe in the early-type galaxies in our SN sample, as listed in Table 5. Hakobyan et al. (2008) carried out a detailed morphological study and an extensive literature search for a sample of 22 CC SNe that had apparently occurred in early-type galaxies, and found a significant fraction (17 out of 22) of these galaxies to actually be misclassified spirals. They also discovered that for the genuine early-type galaxies, there are independent indicators of the presence of recent star formation due to mergers or interactions. As listed in Table 5, the majority of the early-type galaxies with CC SNe in our sample are "S0/a," which is in between S0 and Sa and should have a small amount of recent star formation. The host galaxy of SN 2007ke is classified as "E" in both NED and HyperLeda, but it is interacting with another elliptical galaxy and is a member of a bright cluster of galaxies. The host galaxy of SN 2003ei is classified as "E" in NED, but it occurred in a tidal arm of an interacting galaxy pair. The host galaxy of SN 2005ar is classified as "E" in both NED and HyperLeda; however, we inspected several images from KAIT and DeepSky (Nugent 2009), and suggest that this may be another misclassification because the galaxy does not have a bright nucleus as seen in classical elliptical galaxies and appears to have some diffuse spiral-arm emission.

Thus, we conclude from this exercise that CC SNe in "E" and "S0" galaxies (our galaxy bins 1 and 2) are rare, especially after excluding the ones in "S0/a" galaxies and the misclassifications. The scarcity of CC SNe in the early-type galaxies places a strong limit on the amount of recent star formation within these galaxies, which will be used in Paper III when we discuss possible causes for the observed rate-size relation.

We also note the predominance of SNe Ibc over SNe II in Table 5: of the total 536 CC SNe, only 144 are SNe Ibc (27%), but 7 out of 13 (54%) of the CC SNe in the early-type galaxies are SNe Ibc. In particular, there is a strong preference for the so-called "Ca-rich SNe Ibc" (Filippenko et al. 2003; Perets et al. 2010) to occur in early-type galaxies. About 10 Ca-rich SNe have been identified, all of which were discovered in the LOSS galaxies, and three of them have relatively early-type hosts. As discussed by Perets et al. (2010), the association of Ca-rich SNe Ibc with early-type galaxies provides clues to the nature of their progenitors: they probably represent a new type of stellar explosion arising from a low-mass and relatively old stellar system.

4.2.4   The SN Distribution as a Function of Distance

The left panels of Figure 6 show the distribution as a function of distance for the different types of SNe. SNe Ia, because of their extraordinarily high luminosity, are typically discovered at much greater distances than the CC SNe. The distributions for the SNe Ibc and II are rather similar, reaching a peak at around 50–70 Mpc and displaying a sharp decline after 100–110 Mpc.

The distribution over distance depends on several factors, particularly the SN luminosity, the distribution of Hubble type and galaxy size with distance, and the control time for each galaxy. Because each distance bin has roughly 1000 galaxies, the average control time might be similar in the very nearby distance bins where we have total control during the observing seasons, and then decline in more distant bins when we have only partial control. It is thus possible to estimate at which distance our SN survey has full control for the different SN types.

The right-hand panel of Figure 6 shows how the number of SNe in each distance bin, divided by the total K-band luminosity for *all* galaxies in that bin, evolves with distance. The curves are visually shifted to approximately match the first several distance bins. We expected the curves to show a constant for the nearest distance bins (where the average control times are the same for the different distance bins because we have full control), and then drop for the more distant bins. But instead, the curves exhibit an apparent decline even for the most nearby distance bins. This is the first sign of the presence of a size dependence for the SN rates: even though the average control time may be the same for the very nearby distance bins, the average galaxy size increases significantly with increasing distance (Figure 4), so the average SN rate declines with distance.

Nevertheless, there seems to be a clear divergence between the SN Ia and CC SN curves starting at ~ 70 Mpc. Since SNe Ia are more luminous than the CC SNe, we should have full control of SNe Ia over a larger distance; hence, we take the divergence as a sign that the control time for CC SNe begins to fall short of the total observing season time at distances beyond 70 Mpc. For this reason, and to be conservative, in Paper II we elect to construct our LF sample of CC SNe using a distance cutoff of 60 Mpc (dashed line in Figure 6).

4.2.5   The Radial Distribution of SNe

Our search is conducted with a CCD camera and the SNe are discovered via image subtraction, so the discrimination against SNe occurring near the bright nuclei of galaxies is not as severe as in surveys with photographic plates. Nevertheless, we exclude an area with a radius of a few pixels (3–4, depending on the seeing, corresponding to $2.4''$–$3.2''$) centered on every galaxy nucleus during our search, because galactic nuclei often suffer imperfect image subtraction and introduce many false SN candidates. In order to estimate the fraction of SNe missed as a result of this SN search strategy, we determined the surface density of SNe as a function of radial distance from the center of the host galaxy. In §4.5, we will also perform Monte Carlo simulations to achieve the same goal.

The SNe in our sample have well-documented offsets, x'' east or west and y'' north or south of their host-galaxy nuclei. Under the assumption that the galaxies are circular disks and only appear to have different major and minor axes due to their inclination, we can calculate the radial distance of the SNe (R_{SN}) from the nuclei if we know the position angles and the axis ratios of the galaxies. The radius of the galaxy (R_{gal}) is simply half of the major-axis diameter. The ratio $\theta = R_{SN}/R_{gal}$ is then the fractional radial distance for the SN, and it may be compared for different objects. We group θ in different bins, and calculate the surface density as $N_i/[\pi(\theta_i^2 - \theta_{i-1}^2)]$, where N_i is the number of SNe in bin i.

Figure 7 displays the surface-density distribution versus the fractional radial distance R_{SN}/R_{gal}. The top panel shows the distribution of two SN groups, one with the MaA of the host galaxy greater than $1.25'$ (a total of 433) and the other with smaller host galaxies (a total of 373). The split is designed so that the two distributions are similar for $\theta > 0.3$. The SN distribution in bigger galaxies illustrates that the occurrence of SNe follows an exponential trend, with the highest density in the central regions of galaxies. This is not surprising; the SN occurrence should follow the same trend as the stellar population density in galaxies. The SN distribution in the smaller galaxies, however, shows an apparent change starting at $\theta = 0.25$, and becomes consistently lower at small θ than the measurements for the bigger galaxies. This difference is likely caused by the missing SNe in the central region of the smaller galaxies. Taking the difference in the number of SNe (60) in the two groups as a rough estimate of the missed SNe, about $60/810 \approx 7\%$ of the SNe were missed in our sample. Since our survey likely missed a small fraction of the SNe in the center of the bigger galaxies, the total fraction of SNe missed by our survey is probably $\sim 10\%$. We note that this missed SN fraction is similar to what we derive from Monte Carlo simulations in §4.5 when the detection efficiency of our survey is estimated. We also emphasise that by implementing detection efficiency in the control-time calculation, the missed SN fraction is taken into account when the final rate calculations are performed.

We note that the majority of the ~ 60 SNe missed in our search were not discovered by other SN search groups either. As discussed in §4.2.1, only three reported SNe in the LOSS sample galaxies were missed in our survey because they occurred too close to the nuclei of their host galaxies. Thus, either we have overestimated the number of missed SNe in

our search, or all current SN searches suffer some degree of incompleteness for the SNe in bright galactic nuclei.

It is of interest to check whether the different SN types have different surface-density distributions. The lower panel of Figure 7 shows three curves for SNe Ia, Ibc, and II that are visually shifted to match each other. One notable difference is that there is a dip at small θ values in the SN II distribution. Perhaps SNe II have a higher missed fraction near galaxy nuclei compared to the other two SN types, or SNe II prefer not to occur near galaxy nuclei. On the other hand, SNe Ibc seem to be more concentrated within $\theta < 0.70$ (86% of all) than the other SN types (76% and 71% of all for SNe Ia and II, respectively). To evaluate the significance of these differences, we ran K-S tests on the θ distribution of the SNe, and show the cumulative fractions in Figure 8. Significant differences are found between SNe Ibc and SNe Ia/II, with a respective probability of 2.9% and 1.4% that the SNe come from the same radial distribution.

We checked the above results using SNe in relatively big galaxies (in this case, MaA $> 1.0'$ to maintain a reasonably large sample) to alleviate the effect of missed SNe in the centers of galaxies, and the K-S test probability is (respectively) 9.7% and 5.6%, so there is still a significant difference between SNe Ibc and II. The fact that SNe Ibc prefer to occur at $\theta < 0.70$ possibly indicates a bias toward formation of their progenitors in the higher metallicity regions of galaxies, consistent with what is inferred from the host-galaxy property study in §5.4 of Paper II, where SNe Ibc are found to preferentially occur in more massive (and thus higher metallicity) galaxies than SNe II. We note that a similar metallicity dependence between SNe Ibc and II is reported by Boissier & Prantzos (2009); see also Prantzos & Boissier (2003) and Prieto, Stanek, & Beacom (2008).

We also split the SN Ibc sample into SN Ib and SN Ic subsamples, and show the cumulative fractions of their radial distributions in Figure 8. While no significant difference is found among the SN Ib, Ic, and Ibc samples, the SN Ic sample boasts the most significant difference in radial distribution from the SN II sample; the two samples come from the same population at only 0.1% probability, compared to 15.4% between the SN Ib and SN II samples. The SN Ic sample seems to have the highest central concentration among the core-collapse SNe. This is consistent with the results of Kelly, Kirshner, & Pahre (2008), where SNe Ic were found to have the most significant difference in spatial distribution compared to other core-collapse SNe.

Since the radial distance is only a rough estimate of the location of a SN in its host galaxy, more sophisticated methods are necessary to reveal additional differences in the distribution of the different type of SNe in their host galaxies (e.g., Fruchter et al. 2006; Kelly et al. 2008).

4.3   The Log Files

Numerous log files are assembled as part of our SN search. The telescope observing log files record the details of each observation, including weather conditions, observing parameters such as hour angle and declination, and possible problems. The image-processing log files record all of the details regarding image subtraction and candidate detections.

SN-candidate log files keep track of the history of each SN discovered by our own search, or SNe that were discov-

ered by other groups first but were found by our survey independently at a later time. Part of the goal for keeping these candidate log files is to check whether some of the SN candidates found by the image-processing software are missed by students in our team during the human image-checking process. As detailed in §4.2.1, 304 SNe were independently discovered during our survey, and none of the SNe was missed during the image-checking process. Occasionally, a student would miss a SN candidate during the image checking for a single night, but because we have a short observation interval, the field would be repeated several times with the SN still visible, and it would eventually be noticed by the same student or another student. So, overall, our survey has not missed a single SN due to human error.

Another valuable log file is the observing history of each individual field. Each entry in this log file records the date of the observation, the camera used, the adopted template image, and other potentially relevant information about the image that can be used to derive its limiting magnitude (see details in the next section): the intensity ratio relative to the template image, the sky background, and the seeing as measured by the full width at half-maximum intensity (FWHM) of the stellar images.

One important statistic is the average observation interval for our sample galaxies. A histogram of 2.3 million observations (with typical exposure time of 16 s to 20 s) considered in this rate calculation is shown in Figure 9.[14] The average observation interval is 8.7 d, and the majority ($\sim$ 73%) of the intervals are smaller than 10 d. The histogram also shows a bimodal distribution, with peaks at around 5 d and 9 d. This is the result of our survey strategy: a few hundred very nearby galaxies were set to repeat every 2 d, about 5000 galaxies were set to repeat every 5 d, and the remaining 10,000 galaxies were set to repeat every 10 d. The small observation interval of our search is a major reason why our rates are relatively insensitive to the adopted LF in the control-time calculation, especially for the luminous class of SNe Ia, as discussed in Paper III.

4.4   The Limiting-Magnitude Estimates

The limiting magnitude of the survey images is an important ingredient for the calculation of control times. Historically (e.g., C99), the limiting magnitude was often set as a constant for a particular survey, but in reality, the limiting magnitude for each image is different due to different observing conditions such as clouds, the seeing, and the sky background. We have all of the individual survey images, so in theory we could measure the limiting magnitude for each image, but the data-processing time for over 2 million images is prohibitive. Instead, we derive empirical correlations between the limiting magnitudes for a subset of the images and several parameters recorded in the log files, and apply these correlations to the remaining images.

We find a tight correlation between the limiting magnitude and the logarithm of the intensity ratio (of the search image to the template), the FWHM of stars, and the logarithm of the sky background. We also find that the corre-

lations are different for different combinations of the CCD cameras used to take the image and the template. During the period of our survey that is considered in this rate calculation, we have used three CCD cameras: an Apogee AP7 camera with enhanced ultraviolet coating between March 1998 and Sep. 2001, an Apogee AP7 camera with a broadband coating between Sep. 2001 and May 2007, and a Finger Lakes Instrumentation Proline Camera after May 2007. There are 5 combinations of the cameras used to take the new image and the template.

For each combination, we choose a large number of images (1000–40,000) that were taken under different weather and observing conditions, and derive their limiting magnitudes as follows. All of these images are selected from fields that have either reliable calibrations from our follow-up campaign (Ganeshalingam et al. 2010), or many stars that are calibrated in the USNO B1 catalog (Monet et al. 2003). For each image, artificial stars, with known brightness determined from the calibration and point-spread function (PSF) constructed from bright, isolated stars in the same image, are randomly injected in the image. We then use the "sextractor program" (Bertin & Arnouts 1996) to determine how many of these artificial stars are recovered using a set of default parameters that are also adopted for the candidate detection in the SN search software. We repeat this process with increasingly fainter magnitudes for the artificial stars until > 50% of them are undetected, at which point we set that magnitude as the limiting magnitude of the image. Note that our particular definition of the limiting magnitude is not important, because it is also adopted in our Monte Carlo simulations to determine the detection efficiency, which is eventually used in the rate calculations.

After all of the limiting magnitudes are derived, we use a multiple-variable-regression program to derive the coefficients for the three components mentioned above. Overall, we achieve a solution with a scatter of 0.2–0.3 mag for over 50,000 limiting magnitudes. Figure 10 shows the correlation between the limiting magnitude and the intensity ratio, after the corrections for the other two components (stellar FWHM and sky background) have been made. The overall limiting magnitudes for our survey images spread over a wide range, but are concentrated between 18.0 and 19.5, with a median value of 18.8 ± 0.5 mag.

4.5   The Detection Efficiency

We define the detection efficiency (DE, hereafter) of an image in our survey as the probability of detecting a SN-like point source in that image as a function of the difference between the SN brightness and the limiting magnitude of the image as derived in §4.4. One could assume a step function for the DE (1.0 when the SN is brighter than the limiting magnitude, 0.0 otherwise), but that is only a rough approximation of the real situation; SNe are more likely to be lost in the bright nuclear regions of galaxies, and the limiting magnitude determined in §4.4 is most suitable for isolated stellar sources, not for SNe that are generally superimposed on a host-galaxy background. For this reason, we perform Monte Carlo simulations to determine the DE in our survey, similar to what has been done previously (e.g., Pain et al. 2002; Gal-Yam, Maoz, & Sharon 2002; Blanc et al. 2004; Neill et al. 2006; Sullivan et al. 2006; Sharon et al. 2007).

---

[14] We do not consider the long interval when a galaxy is too near the direction to the Sun for observations.

In an attempt to investigate whether the DE is correlated with the properties of the galaxies, we select 34 galaxies having different Hubble types and sizes. For each galaxy, we choose several images that were observed under different observing conditions so that we have good coverage of the limiting magnitudes. A total of 189 images are selected to participate in the simulations. Additional images of more galaxies are in principle desirable to sample the total range of galaxy morphology and observing conditions, but the DE simulation is a time-consuming process (in both computation and analysis), and we reach the point of diminishing returns as the DE curves converge toward the same galaxy Hubble type (see discussion below).

We follow the prescription of Gal-Yam et al. (2002) to inject simulated SNe into the images, with a spatial distribution that follows the flux of the galaxy. For this purpose, we construct deep template images for each of the 34 galaxies by stacking the images observed under the best conditions. Stars that are within the galaxy profiles are carefully removed by modelling their PSFs. The remaining flux maps of the galaxies are used as the probability maps where the simulated SNe should be located. We emphasize that the simulated SN injection process does not avoid the nuclear region of a galaxy. Quite the contrary, the nuclear region usually has the highest flux of the galaxy so it has the highest possibility (per unit area) of harboring a simulated SN.

For each image, we study the detection efficiency for SNe that are from 2 mag brighter to 1 mag fainter than the limiting magnitude, using a 0.2 mag increment. For each SN magnitude, 20 simulated SNe are randomly injected into the image one at a time according to the flux map. The image is then processed with the same software used in our SN search to do template image subtraction and SN candidate detection. As in the case of our actual search, the central few pixels in the nuclear region of a galaxy are excluded. The SN candidate positions are checked against the input coordinates of the simulated SNe to determine whether they are recovered. The efficiency derived in this manner then naturally accounts for parts of the image that are not useable for the SN search, such as the central several pixels in the bright galaxy nucleus (because the simulated SNe are injected there according to the galaxy flux maps, but the image-processing software excludes these regions in both our actual search and the simulations).

Our DE results are shown in Figure 11. We find that the DE curves do not change significantly for different limiting magnitudes, but show a strong dependence on the Hubble types of the galaxies. The curves are flat when the SN magnitude is brighter than the limiting magnitude by more than 1 mag, then have a dramatic drop when the SN is 0.5 mag fainter than the limiting magnitude, and reach zero when the SN is 1 mag fainter than the limiting magnitude. At any given SN magnitude, the early-type galaxies (E–S0) have the lowest DE while the late-type galaxies (Scd–Irr) have the highest DE, due to the presence of bright nuclear regions in the early-type galaxies that tend to obscure SNe. In fact, this becomes a serious issue for early-type galaxies having small sizes. As shown in the inset of Figure 11, the early-type galaxies with MaA smaller than $1'$ have rather poor DE even when the detection is not limited by the brightness of the SNe. As discussed in Papers II and III, we eliminated

the small early-type galaxies and the associated SNe in our final rate calculations by using the "optimal" subsamples.

The Monte Carlo simulations suggest that $\sim 10\%$ of the SNe with magnitudes much brighter than the limiting magnitude are missed in the nuclear regions of the galaxies due to our SN search strategy, which is consistent with the estimate from the radial distribution of the SNe. The detection efficiency takes into account this missed fraction, so our final rates are not affected.

5   CONCLUSIONS

This is Paper I of a series aiming to determine the rates of different types of SNe in nearby galaxies, using data obtained from the Lick Observatory Supernova Search during the past decade. Here, we first provide an outline of the series (§2.1), discuss the improvements of our rate calculations over published results (§2.2), and explore possible limitations (§2.3).

We then provide a mathematical derivation for the control-time calculation for a SN type having a known luminosity function (LF) represented by discrete components, with details in the Appendix. Not surprisingly, the total control time is the sum of the control times for each SN weighted by its fraction in the LF.

We provide details on the construction of our total galaxy sample and the different galaxy subsamples. Although our total galaxy sample has a strong deficit of low-luminosity galaxies, the galaxy sample within 60 Mpc is representative of a complete galaxy sample for $L_K \gtrsim 7 \times 10^{10}\,\mathrm{L}_\odot$. Moreover, there is a sufficiently large number of faint galaxies in our sample to provide good statistics for the rate calculations (as demonstrated in Paper III). We also discuss the properties of our sample galaxies and their change over distance. There is a strong Malmquist bias, so the low-luminosity galaxies become increasingly incomplete, leading to a monotonic increase in the average galaxy size with increasing distance. This is an important trend that will be used in Paper III to demonstrate a correlation between the SN rates and galaxy sizes.

The construction of the SN sample is discussed. In total, 1036 SNe were found directly or independently by LOSS in the LOSS fields, and 929 were discovered in the galaxies considered for the rate calculations. Several SN subsamples are constructed, an important one of which excludes all SNe that occurred in small (MaA $< 1'$), early-type galaxies and in highly inclined ($i > 75°$) spiral galaxies; it has 726 SNe and is the "optimal" subsample for the final rate calculation. We also confirm a significant difference between the Hubble-type distributions of SNe Ia and CC SNe, as we had reported previously (van den Bergh et al. 2002, 2003, 2005). A small number of CC SNe ($< 3\%$) were found in early-type galaxies, mostly in S0/a galaxies that probably have low-level, recent star formation. The host galaxies of the remaining CC SNe show other signs of recent star formation, or are misclassified spirals. Hence, CC SNe in E–S0 galaxies are very rare, and this places a strong limit on the amount of recent star formation in these galaxies. We also find that the subclass of subluminous, peculiar, "Ca-rich SNe Ibc" have a high fraction in early-type galaxies, consistent with

recent suggestions that they come from low-mass stars in old populations (Perets et al. 2010).

Details on the log files, and on how the limiting magnitude of each image is calculated from information in the log files, are provided. The limiting magnitude is a function of the intensity ratio of the new and template images, the stellar FWHM, and the sky background. Our limiting magnitude can be measured to a precision of 0.2–0.3 mag for any individual image in the survey. We also show that for the more than 2 million observations considered in this SN rate calculation, the average observation interval is ~ 9 d, which in most cases is much smaller than the control time for the different types of SNe. Consequently, the contribution to the control time is often the observation intervals themselves (multiplied by the detection efficiency). This ensures that our control times have a great degree of tolerance to uncertainties in the SN LFs.

We perform Monte Carlo simulations to study the detection efficiency (DE) in our survey. Simulated SNe with different brightness are injected into the images, which are then processed with the SN search software used in our survey to study the fraction of the recovered SNe. We find that the DE curves are different for galaxies of different Hubble types, with the early-type galaxies having the lowest DE and the late-type galaxies having the highest DE. This is probably caused by the higher missed fraction of SNe in the brighter nuclei of the early-type galaxies. Overall, $\sim 10\%$ of the injected bright SNe are missed in the simulations due to our search strategy, consistent with an estimate from a study of the radial distribution of SNe. The DE curves take into account this missed fraction in the final rate calculations.

It is demonstrated that the very nearby LOSS galaxies (within 60 Mpc) are representative of galaxies bigger than the Milky Way, but include many faint galaxies as well (though with an apparent deficit compared to the complete sample). There are abundant galaxies of different Hubble types within 60 Mpc (Figures 2 and 4), and our survey may have nearly full control over the different types of SNe in these galaxies (Figure 6). In Paper II, we will construct LFs for the CC SNe using SNe discovered in these nearby LOSS galaxies. Because of their extreme brightness, our survey is complete for SNe Ia to a greater distance, so the cutoff distance is set at 80 Mpc.

After deriving the limiting magnitude and the detection efficiency for any individual image in our survey, we need two additional pieces of information to calculate the control time for any given type of SN: the distribution of the intrinsic brightness of SNe (i.e., the LF) and their light-curve shapes. These are the main results from Paper II, where for the first time a complete SN sample is constructed and the observed LFs are derived.

ACKNOWLEDGMENTS

REFERENCES

Arcavi I., et al. 2010, ApJ, 721, 777

Barris B. J., Tonry J. L. 2006, ApJ, 637, 427

Benetti S., et al. 2005, ApJ, 623, 1011

Bertin E., Arnouts, S. 1996, A&AS, 117, 393

Bildsten L., Shen K. J., Weinberg N. N., Nelemans G. 2007, ApJ, 662, L95

Blanc G., et al. 2004, A&A, 423, 881

Blondin S., Tonry J. L. 2007, ApJ, 666, 1024

Boissier S., Prantzos N. 2009, A&A, 503, 137

Botticella M. T., et al. 2008, A&A, 479, 49

Bottinelli L., Gouguenheim L., Paturel G., Teerikorpi P. 1995, A&A, 296, 64

Branch D., Tammann G. A. 1992, ARA&A, 30, 359

Brinchmann J., Charlot S., White S. D. M., Tremonti C., Kauffmann G., Heckman T., Brinkmann J. 2004, MNRAS, 351, 1151

Cappellaro E., Evans R., Turatto M. 1999, A&A, 351, 459 (C99)

Cappellaro E., Turatto M. 1988, A&A, 190, 10

Cappellaro E., Turatto M., Benetti S., Tsvetkov D. Y., Bartunov O. S., Makarova I. N. 1993a, A&A, 268, 472

Cappellaro E., Turatto M., Benetti S., Tsvetkov D. Yu., Bartunov O. S., Makarova I. N. 1993b, A&A, 273, 383

Cappellaro E., Turatto M., Tsvetkov D. Yu., Bartunov O. S., Pollas C., Evans R., Hamuy M. 1997, A&A, 322, 431

Cardelli J. A., Clayton G. C., Mathis J. S. 1989, ApJ, 345, 245

Connolly A. 2004, IAU Circ., 8359, 1

Dahlen T., Strolger L.-G., Riess A. G. 2008, ApJ, 681, 462

Dahlen T., et al. 2004, ApJ, 613, 189

Della Valle M., Panagia N., Padovani P., Cappellaro E., Mannucci F., Turatto M. 2005, ApJ, 629, 750

de Vaucouleurs G., de Vaucouleurs A., Corwin J. R. 1976, Second Reference Catalogue of Bright Galaxies (Austin: University of Texas Press)

de Vaucouleurs G., de Vaucouleurs A., Corwin H. G. Jr., Buta R. J., Paturel G., Fouque P. 1991, Third Reference Catalogue of Bright Galaxies (Springer-Verlag: New York) (RC3)

Dilday B., et al. 2008, ApJ, 682, 262

Dilday B., et al. 2011, in prep.

Drake A. J., et al. 2009, ApJ, 696, 870

Filippenko A. V. 1997, ARA&A, 35, 309

Filippenko A. V. 2003, in From Twilight to Highlight: The Physics of Supernovae, ed. W. Hillebrandt & B. Leibundgut (Berlin: Springer-Verlag), 171

Filippenko A. V. 2005a, in The Fate of the Most Massive Stars, ed. R. Humphreys & K. Stanek (San Francisco: ASP), 33

Filippenko A. V. 2005b, in White Dwarfs: Cosmological and Galactic Probes, ed. E. M. Sion, S. Vennes, & H. L. Shipman (Dordrecht: Springer), 97

Filippenko A. V., Chornock R. 2002, IAU Circ., 7825, 1

Filippenko A. V., Chornock R., Swift B., Modjaz M., Simcoe R., Rauch M. 2003, IAU Circ., 8159, 2

Filippenko A. V., Foley R. J., Silverman J. M., Chornock R., Li W., Blondin S., Matheson T. 2007, CBET, 926, 1

Filippenko A. V., Li W., Treffers R. R. 2011, in prep.

Filippenko A. V., Li W., Treffers, R. R., Modjaz M. 2001, in Small-Telescope Astronomy on Global Scales, ed. W. P. Chen, C. Lemme, & B. Paczyński (San Francisco: ASP), 121

Filippenko A. V., et al. 1992a, ApJ, 384, L15

Filippenko A. V., et al. 1992b, AJ, 104, 1543

Foley R. J., Smith N., Ganeshalingam M., Li W., Chornock R., Filippenko A. V. 2007, ApJ, 657, L105

Foley R. J., et al. 2009, AJ, 138, 376

Foley R. J., et al. 2010, ApJ, 708, L61

Fruchter A. S., et al. 2006, Nature, 441, 463

Gal-Yam A., Maoz D., Sharon K. 2002, MNRAS, 332, 37

Gal-Yam A., Poznanski D., Maoz D., Filippenko A. V., Foley R. J. 2004, PASP, 116, 597

Ganeshalingam M., et al. 2010, ApJS, 190, 418

Graham J., Li W. 2003, IAU Circ., 8115, 2

Hakobyan A. A., Petrosian A. R., McLean B., Kunth D., Allen R. J., Turatto M., Barbon R. 2008, A&A, 488, 523

Hamuy M., Maza J., Folatelli G. 2005, CBET, 260, 1

Hardin D., et al. 2000, A&A, 362, 419

Horesh A., Poznanski D., Ofek E. O., Maoz D. 2008, MNRAS, 389, 1871

Hubble E. P. 1926, ApJ, 64, 321

Jarrett T. H., Chester T., Cutri R., Schneider S. E., Huchra J. P. 2003, AJ, 125, 525

Jha S., Branch D., Chornock R., Foley R. J., Li W., Swift B. J., Casebeer D., Filippenko A. V. 2006, AJ, 132, 189

Kelly P. L., Kirshner R. P., Pahre M. 2008, ApJ, 687, 1201

Kinugasa K., Kawakita H., Yamaoka H., Naito H. 2002, IAU Circ., 7844, 4

Kochanek C. S., et al. 2001, ApJ, 560, 566

Le Borgne D., Rocca-Volmerange B., Prugniel P., Lançon A., Fioc M., Soubiran C. 2004, A&A, 425, 881

Leibundgut B., Tammann G. A., Cadonau R., Cerrito D. 1991, A&AS, 89, 537

Leibundgut B., et al. 1993, AJ, 105, 301

Li W. 2005, IAU Circ., 8647, 1

Li W., Filippenko A. V., Mostardi R., Chornock R., Foley R. J., Smith N. 2008, CBET, 1265, 1

Li W., Filippenko A. V., Treffers R. R., Riess A. G., Hu J., Qiu Y. 2001, ApJ, 546, 734

Li W., Singer D., Boles T. 2004, IAU Circ., 8361, 1

Li W., et al. 2000, in Cosmic Explosions, ed. S. S. Holt & W. W. Zhang (New York: AIP), 103

Li W., et al. 2003, PASP, 115, 453

Li W., et al. 2011a, MNRAS, submitted (arXiv:1006.4612) (Paper II)

Li W., Chornock R., Leaman J., Filippenko A. V., Poznanski D., Wang X., Ganeshalingam M., Mannucci F. 2011b, MNRAS, submitted (arXiv:1006.4612) (Paper III)

Madgwick D. S., Hewett P. C., Mortlock D. J., Wang L. 2003, ApJ, 599, L33

Mannucci F., Della Valle M., Panagia N., Cappellaro E., Cresci G., Maiolino R., Petrosian A., Turatto M. 2005, A&A, 433, 807 (M05)

Mannucci F., Della Valle M., Panagia N. 2006, MNRAS, 370, 773

Mannucci F., Maoz D., Sharon K., Botticella M. T., Della Valle M., Gal-Yam A., Panagia N. 2008, MNRAS, 383, 1121

Maoz D., Mannucci F., Li W., Filippenko, A. V., Della Valle M., Panagia N. 2011, MNRAS, in press (Paper IV) (arXiv:1002.3056)

Miller A. A., et al. 2009, ApJ, 690, 1303

Modjaz M., Kirshner R., Challis P., Blondin S., Berlind P. 2005, IAU Circ., 8650, 2

Modjaz M., et al. 2008, AJ, 135, 1136

Monet D. G., et al. 2003, AJ, 125, 984

Neill J. D., et al. 2006, AJ, 132, 1126

Nugent P. E. 2009, BAAS, 41, 419

Ochsenbein F., Bauer P., Marcout J. 2000, A&AS, 143, 23

Pain R., et al. 2002, ApJ, 577, 120

Pastorello A., et al. 2007, Nature, 447, 829

Paturel G., Petit C., Prugniel P., Theureau G., Rousseau J., Brouty M., Dubois P., Cambrésy L. 2003, A&A, 412, 45

Perets H. B., et al. 2010, Nature, 465, 322

Perlmutter S., et al. 1999, ApJ, 517, 565

Phillips M. M., Wells L. A., Suntzeff N. B., Hamuy M., Leibundgut B., Kirshner R. P., Foltz C. B. 1992, AJ, 103, 1632

Poznanski D., Gal-Yam A., Maoz D., Filippenko A. V., Leonard D. C., Matheson T. 2002, PASP, 114, 833

Poznanski D., Maoz D., Gal-Yam A. 2007, AJ, 134, 1285

Poznanski D., et al. 2007, MNRAS, 382, 1169

Poznanski D., et al. 2010, Science, 327, 58

Prantzos N., Boissier S. 2003, A&A, 406, 259

Prasad R. R., Shimasaki K., Lee E., Li W. 2005, IAU Circ., 8616, 2

Prieto J. L., Stanek K. Z., Beacom J. F. 2008, ApJ, 673, 999

Pskovskii Yu. P. 1961, AZh, 38, 656

Pskovskii Yu. P. 1967, Soviet Astronomy, 11, 63

Quimby R. 2006, CBET, 644, 1

Quimby R. M., et al. 2009, Nature, submitted (arXiv:0910:0059)

Rajala A., Fox D. B., Gal-Yam A. 2004, The Astronomer's Telegram, 320, 1

Rajala A. M., et al. 2005, PASP, 117, 132

Richardson D., Branch D., Casebeer D., Millard J., Thomas R. C., Baron E. 2002, AJ, 123, 745

Richmond M., Treffers R. R., Filippenko A. V. 1993, PASP, 105, 1164

Riess A. G., et al. 1998, AJ, 116, 1009

Riess A. G., et al. 2009, ApJ, 699, 539

Scannapieco E., Bildsten L. 2005, ApJ, 629, L85

Schlegel D. J., Finkbeiner D. P., Davis M. 1998, ApJ, 500, 525

Schwartz M., Li W., Filippenko A. V., Modjaz M., Treffers R. R. 2000, IAU Circ., 7514, 2

Serduke F. J. D., Blum A., Scala J., Filippenko A. V., Chornock R. 2006, CBET, 380, 1

Sharon K., Gal-Yam A., Maoz D., Filippenko A. V., Guhathakurta P. 2007, ApJ, 660, 1165

Spergel D. N., et al. 2007, ApJS, 170, 377

Strolger L.-G., et al. 2004, ApJ, 613, 200

Sullivan M., et al. 2006, ApJ, 648, 868

Tonry J. L., et al. 2003, ApJ, 594, 1

van den Bergh S. 1988, PASP, 100, 344

van den Bergh S. 1991, Phys. Rep., 204, 385

van den Bergh, S., McClure R. D. 1990, ApJ, 359, 277

van den Bergh S., Li W., Filippenko A. V. 2002, PASP, 114, 820

van den Bergh S., Li W., Filippenko A. V. 2003, PASP, 115, 1280

van den Bergh S., Li W., Filippenko A. V. 2005, PASP, 117, 773

van den Bergh S., McClure R. D., Evans R. 1987, ApJ, 323, 44

Valenti S., et al. 2009, Nature, 459, 674

Van Dyk S. D., Peng C. Y., King J. Y., Filippenko A. V., Treffers R. R., Li W., Richmond M. W. 2000, PASP, 112, 1532

Wang X., et al. 2009, ApJ, 699, L139

Wei J. Y., Qiu Y. L., Cao H. L., Wang J., Hu J. Y. 2002, IAU Circ., 7861, 1

Wheeler J. C., Harkness R. P. 1990, Rep. Prog. Phys., 53, 1467

Zwicky F. 1938, ApJ, 88, 529

Zwicky F. 1942, ApJ, 96, 28
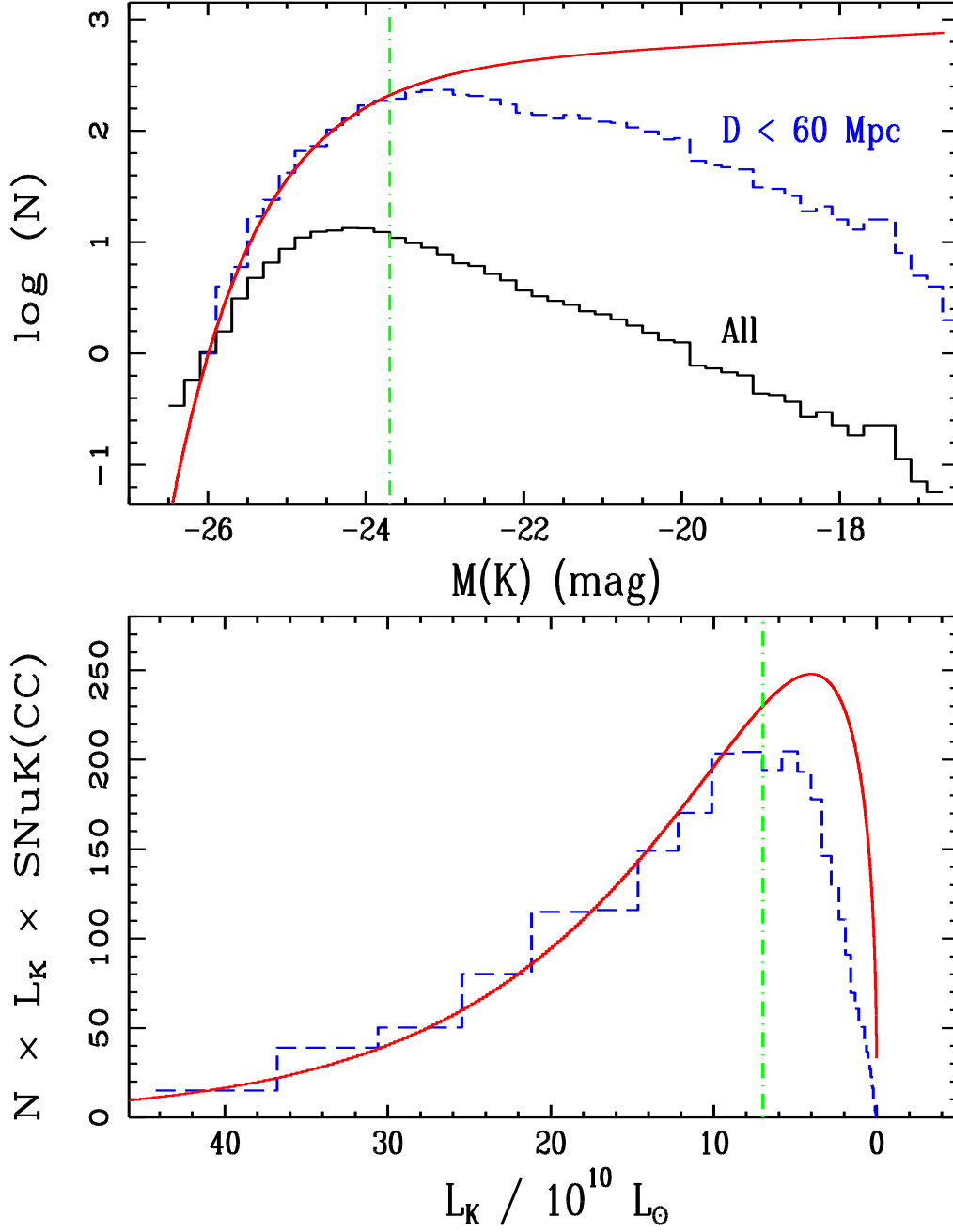
Figure 1. *Upper panel:* K-band luminosity function for all of the LOSS galaxies (solid steps) and for the LOSS galaxies within 60 Mpc (dashed steps) versus the galaxy luminosity function for a complete sample (smooth curve; Kochanek et al. 2001). *Lower panel:* The effective contribution to the number of CC SNe for each luminosity bin. The curves represent the same samples as in the upper panel, except that the curve for the "full" sample is not shown. In both panels, the dot-dashed line marks the nominal galaxy size ($L_K = 7 \times 10^{10}$ L$_\odot$) used for the final rate calculation in Paper III.
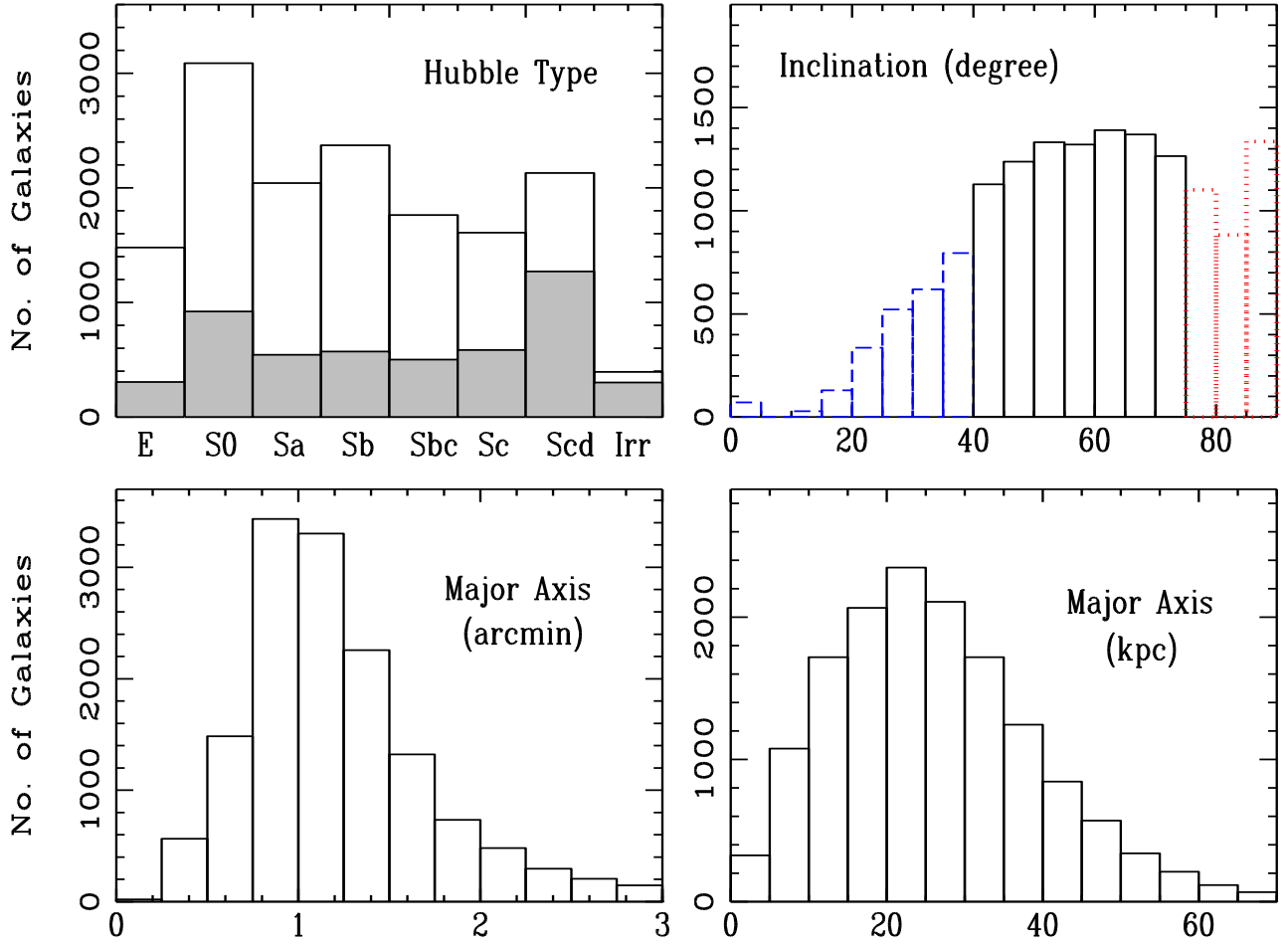
Figure 2. Some statistics regarding the LOSS galaxy sample. *Upper left*: the Hubble-type distribution for all of the galaxies (open histogram) and for galaxies within 60 Mpc (shaded histogram). *Upper right*: the distribution of the inclination angles. The inclination angles are broadly categorised into three bins: face-on (dashed line), normal inclination (solid line), and edge-on (dotted line). *Lower left*: the size (MaA, in arcmin) distribution of the galaxies. *Lower right*: the size (MaA, in kpc) distribution of the galaxies.
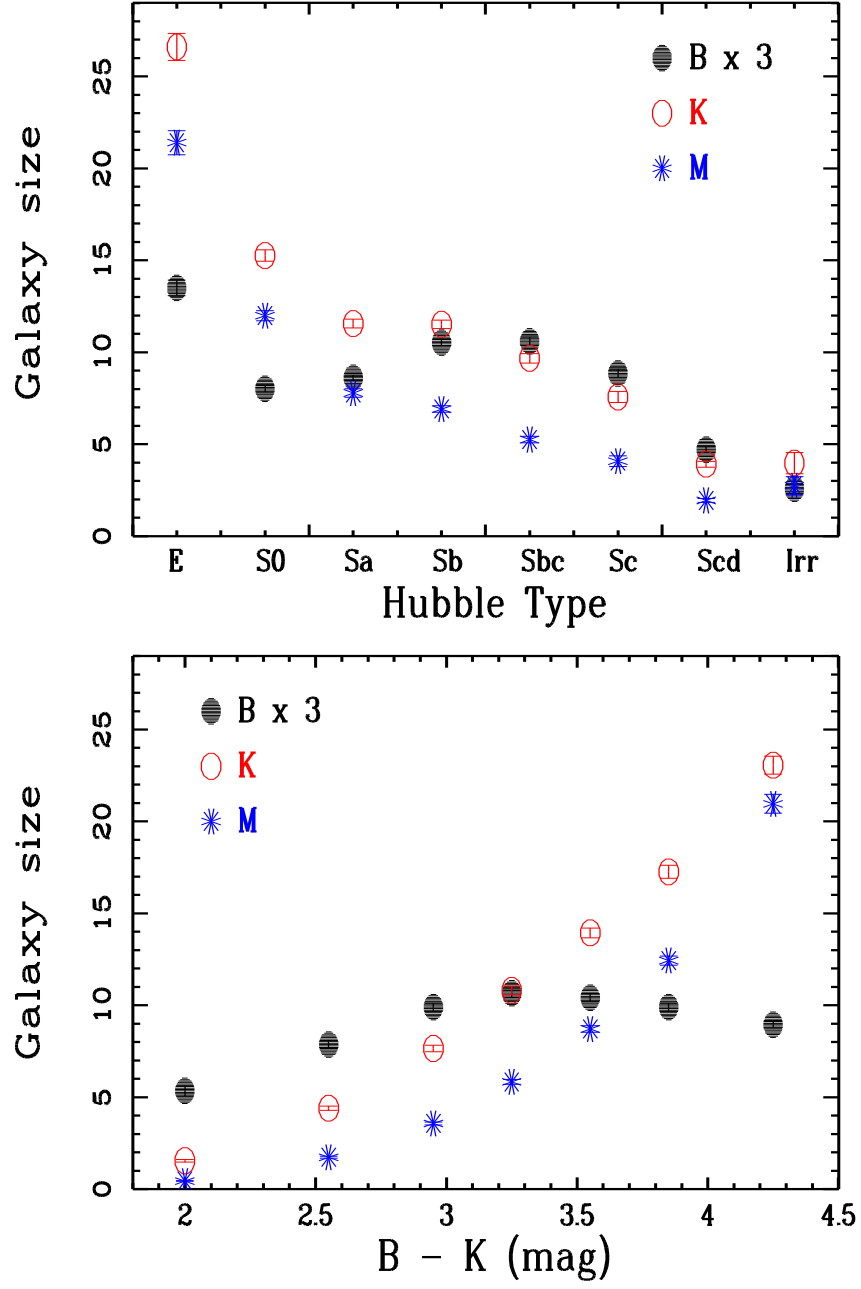
**Figure 3.** The average size of the galaxies versus galaxy Hubble type and $B - K$ colour. For the B and K luminosity, the size is in units of 10×10^{10} $L_{\odot}$, while for the mass, the size is in units of 10×10^{10} $M_{\odot}$.
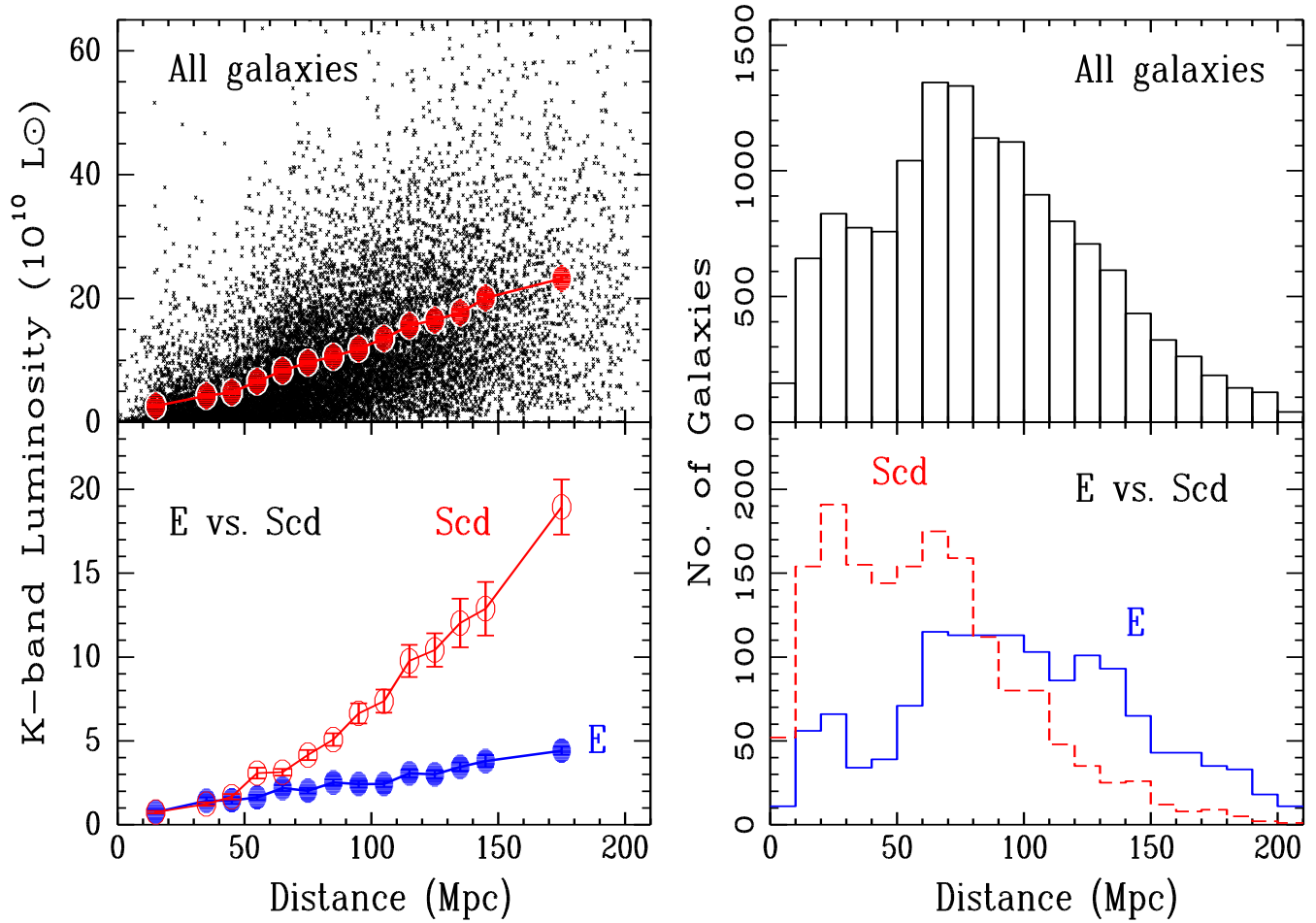
Figure 4. The change of the LOSS galaxy properties over distance. The upper-left panel shows the *K*-band luminosity. Each dot represents a galaxy, while the average luminosity in different distance bins is overplotted as big solid dots connected by a line. The lower-left panel shows the change of the average *K*-band luminosity over distance for two galaxy Hubble types. The Scd galaxies have a more dramatic change than do the E galaxies. The upper-right panel shows the number distribution for all of the galaxies over distance, while the lower-right panel shows this for two different Hubble types.
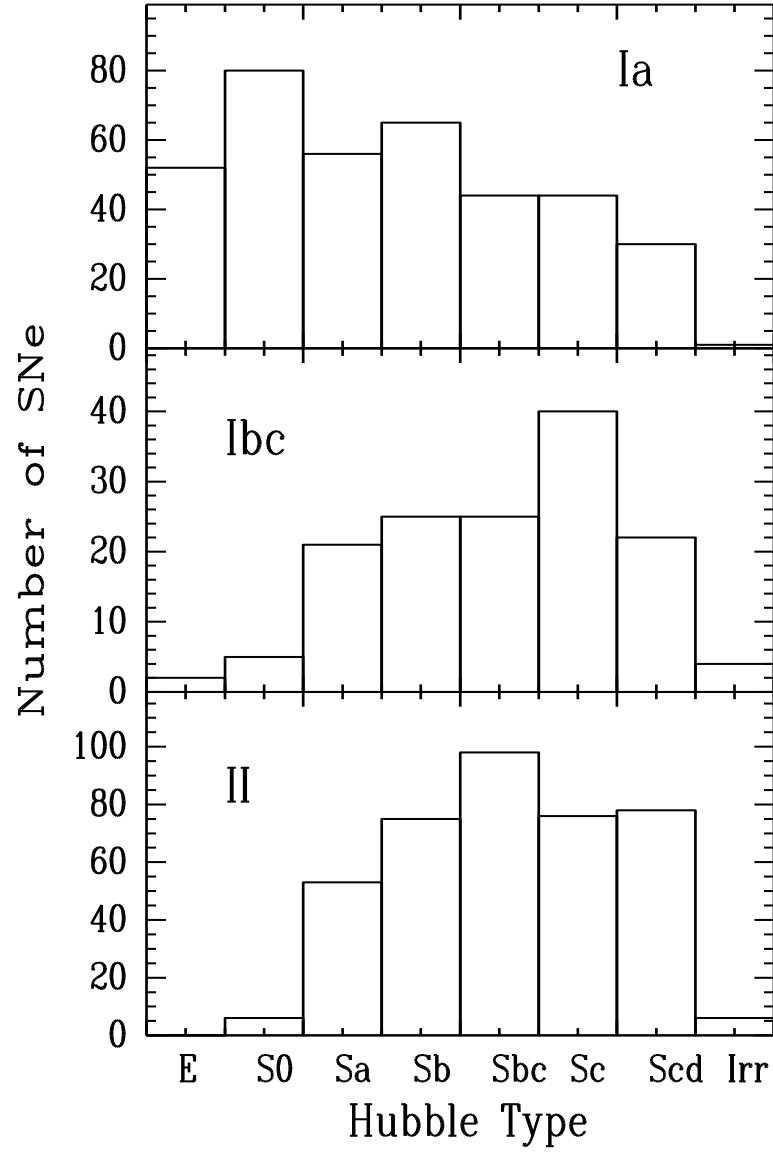
Figure 5. The Hubble-type distribution for the host galaxies of different types of SNe. There is a significant difference between the distribution of SN Ia hosts and SN Ibc/II hosts, while the SN Ibc and SN II hosts have similar distributions.
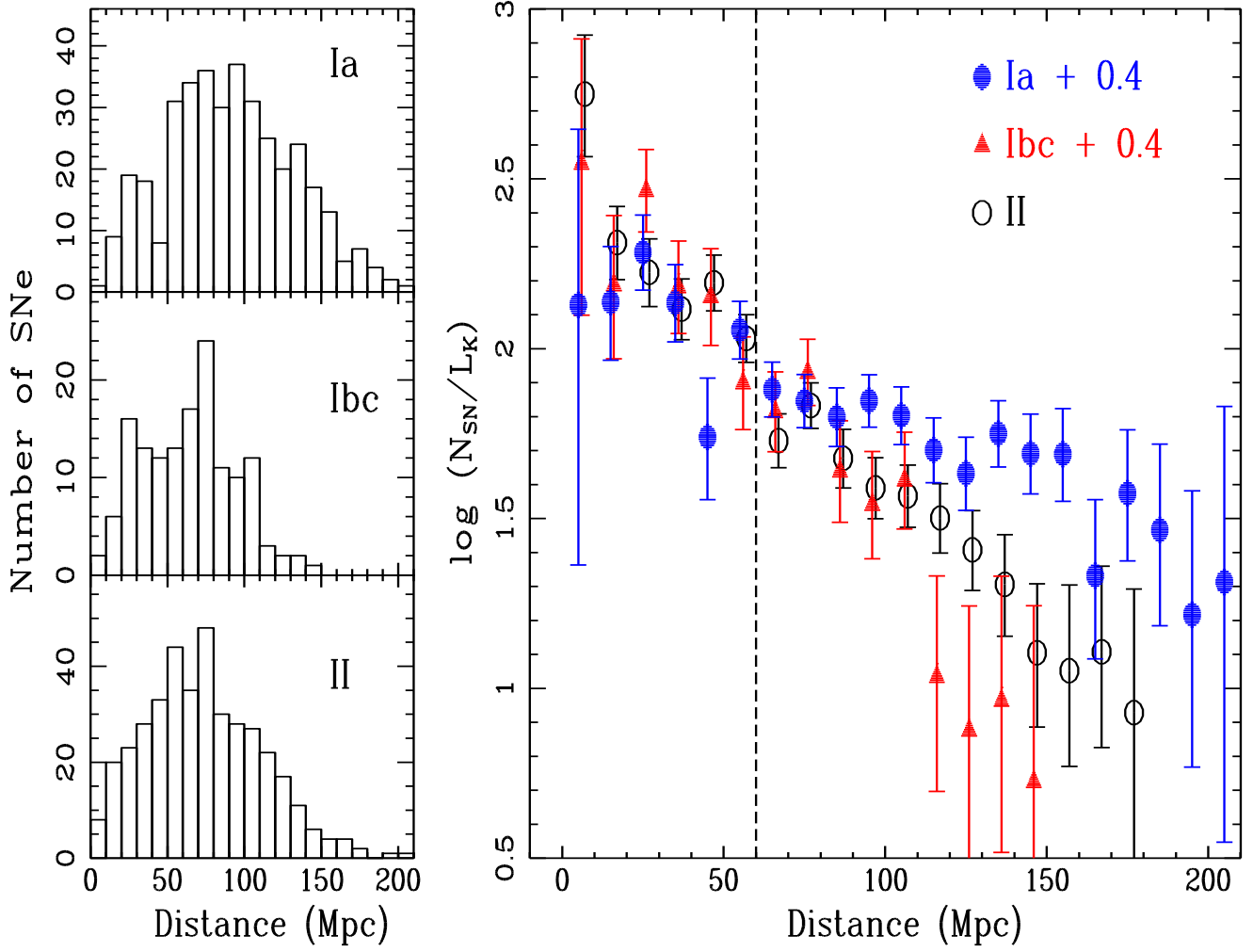
Figure 6. The left panels show the distribution of SNe over distance. The right panel shows the ratio of the number of SNe in each bin divided by the total K-band luminosity for all the galaxies in the same distance bin.
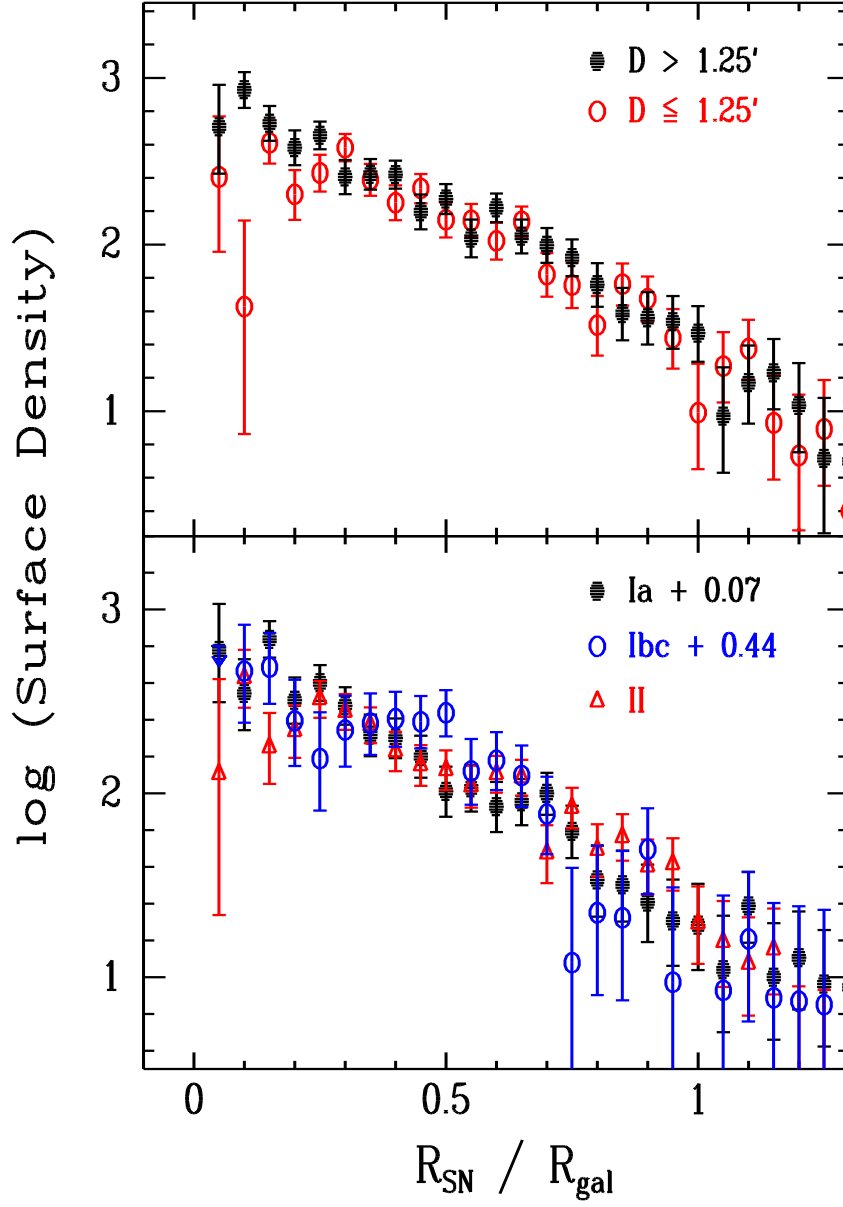
Figure 7. The radial distribution of SNe in their host galaxies. The upper panel shows the distribution for two groups of SNe, one with relatively large host galaxies (MaA > 1.25′) and the other with smaller galaxies. The lower panel shows the radial distribution for different types of SNe.
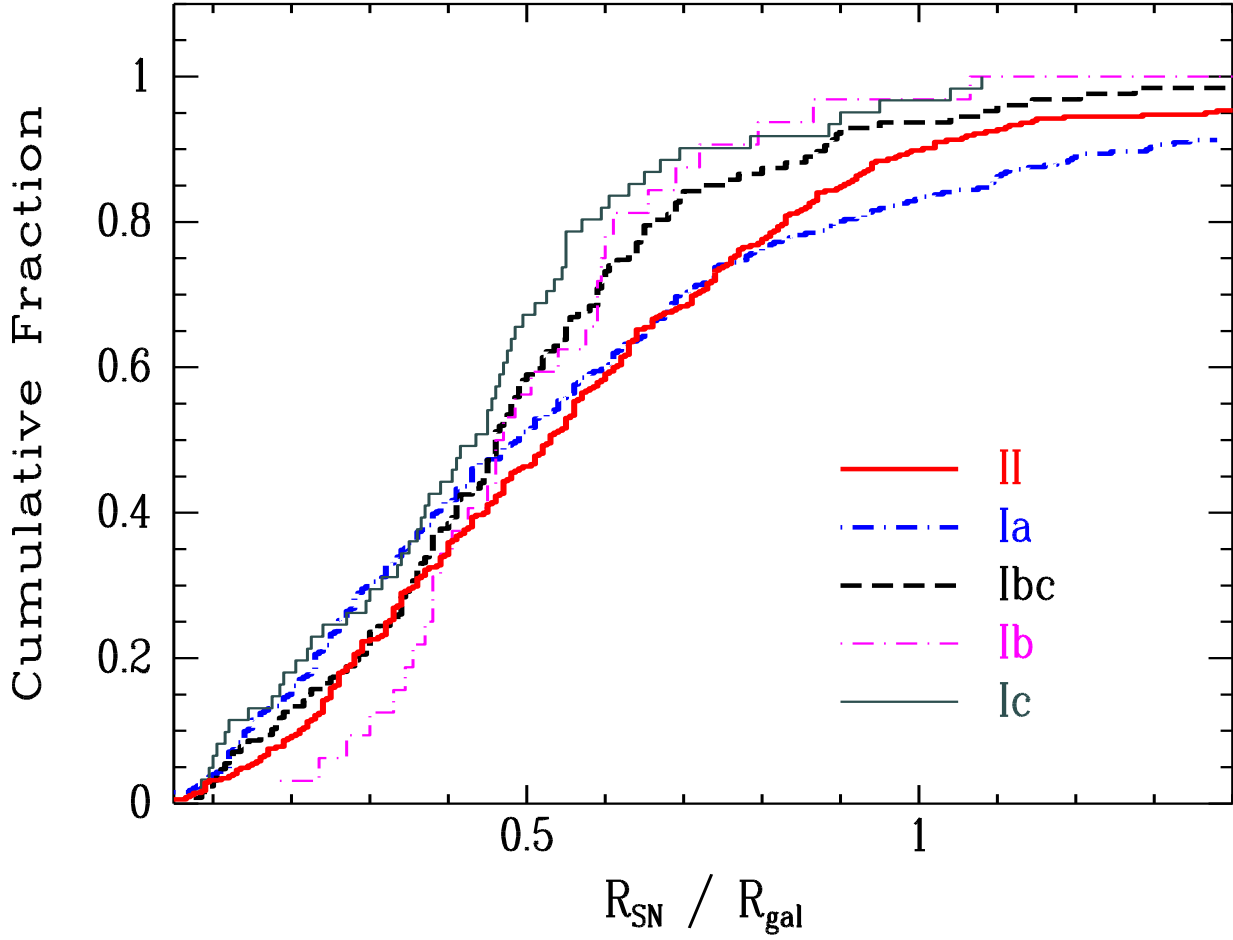
Figure 8. The cumulative fractions for the radial distributions of SNe Ia (thick dash-dotted line), Ibc (thick dashed line), II (thick solid line), Ib (thin dash-dotted line), and Ic (thin solid line).
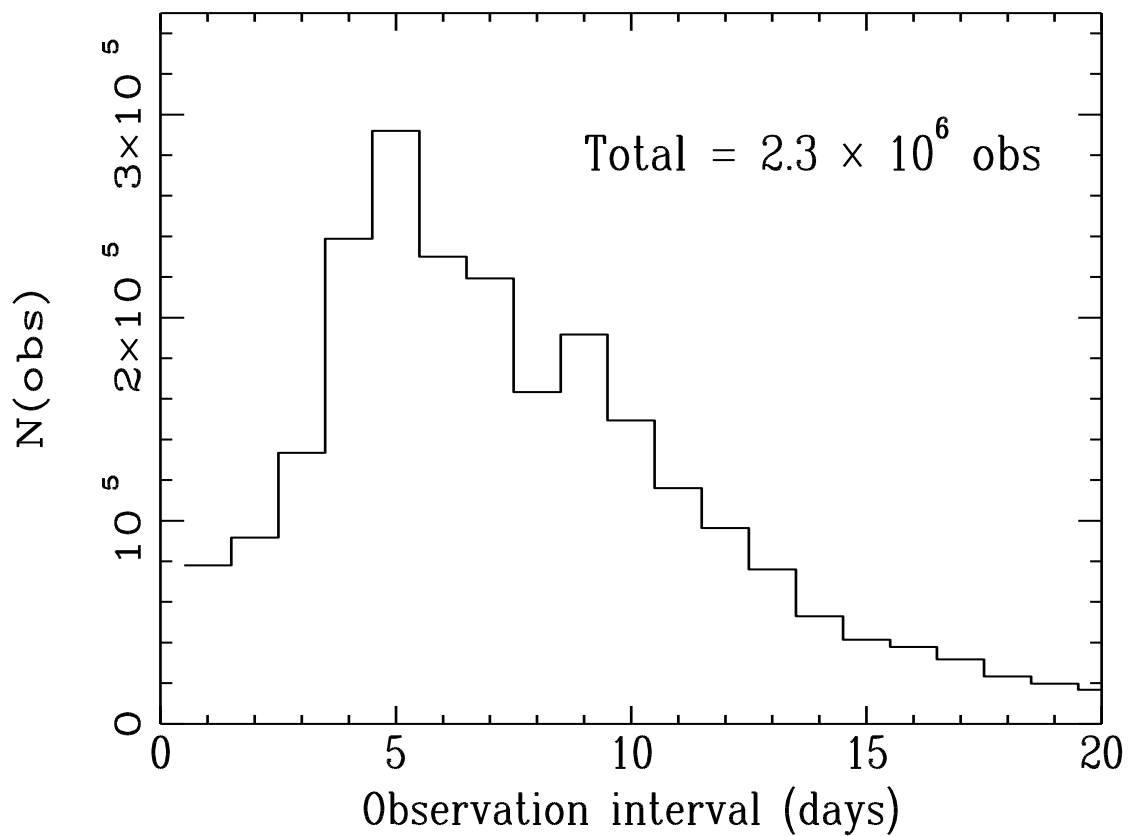
Figure 9. The distribution of the observation intervals for over 2 million observations considered in the current SN rate calculation.
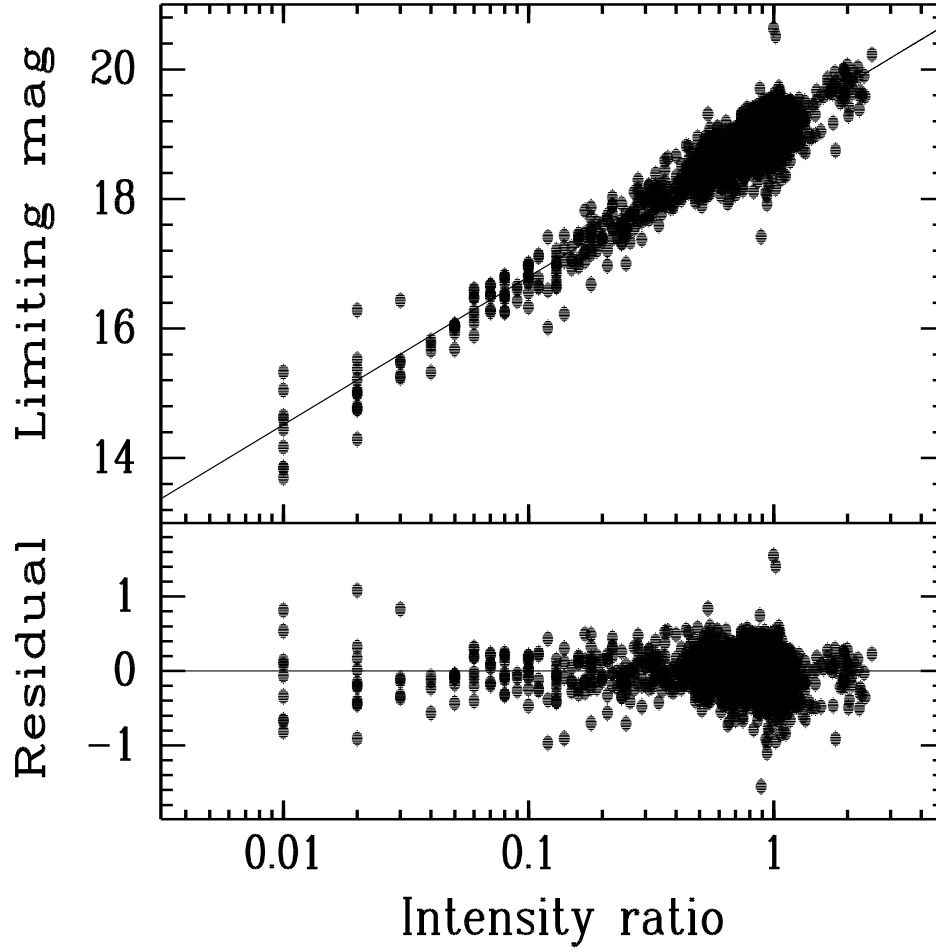
Figure 10. The correlation between the limiting magnitudes and the intensity ratio between the search image and the template. The limiting magnitudes have been corrected for the FWHM and sky background of the images to highlight the correlation shown here.
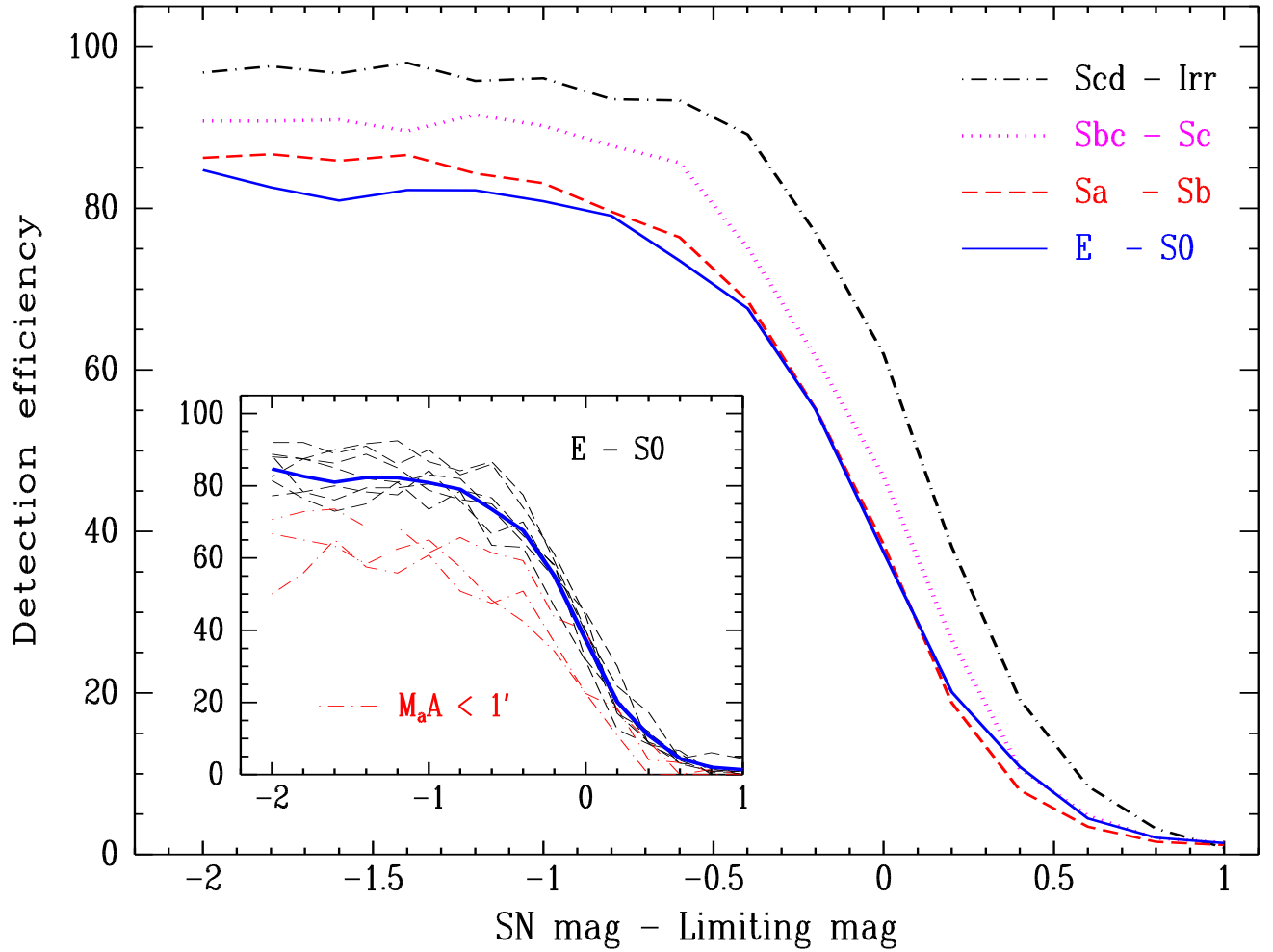
Figure 11. The detection efficiency (DE) in our survey. The DE curves have a strong dependence on the galaxy Hubble type, with the late-type galaxies having the highest DE and the early-type galaxies having the lowest DE. The inset shows the construction of the DE curve for the E–S0 galaxies. Each dashed line is the DE curve for one galaxy. The dash–dotted lines are for galaxies with small sizes (MaA < 1′), and they are not included in calculating the average DE curve (thick line).

Table 1. Hubble-type definitions.

Number[a]	Symbol[b]	Type	T^c
1	E	E, E–S0	-5 to -3
2	S0	S0, S0a	-2 to 0
3	Sa	Sa, Sab	1 to 2
4	Sb	Sb	3
5	Sbc	Sbc	4
6	Sc	Sc	6
7	Scd	Scd, Sd, Sm	7 to 9
8	Irr	Irr	10

[a] The number sequence for the Hubble types used in this study.
[b] The symbols used in all of the figures.
[c] The range of T values, a numerical code for the Hubble types as defined by RC3.

Landscape Table 2 to go here.

Table 2. Galaxy properties in the LOSS "full" sample.

Landscape Table 3 to go here.

Table 3. Average galaxy properties in the "full" and "optimal" samples.

Landscape Table 4 to go here.

Table 4. The supernova sample.

Table 5. Core-collapse SNe in early-type galaxies.

SN	Type	Host	NED	HyperLeda	H2008	Comment
1999ew	II	NGC-3677	S0/a	S0/a	...	
2000ds	Ibcp	NGC-2768	S0/a	E	S0	"Ca-rich"
2002aq	II	MCG-01-7-35	S0	S0/a	...	SN in a star-forming ring
2003ei	IIn	UGC-10402	...	E	...	SN in a tidal arm
2004gh	II	MCG-04-25-6	S0/a	S0/a	...	
2005E	Ibcp	NGC-1032	S0/a	S0/a	...	"Ca-rich"
2005ar	Ib	CGCG-011-033	E	E	...	Possible S0/a galaxy
2005lw	II	IC-672	...	S0/a	...	
2006ee	II	NGC-774	S0	S0	S0	
2006lc	Ib	NGC-7364	S0/a	S0/a	...	
2007aw	Ic	NGC-3072	S0/a?	S0/a	...	
2007ke	Ibcp	NGC-1129	E	E	...	In a cluster; "Ca-rich"
2007kj	Ibc	NGC-7803	S0/a	S0/a	...	

APPENDIX A: DETAILS OF THE CONTROL-TIME METHOD

The control-time method is used in our rate calculations. Here we first describe how the method is implemented in the most basic scenario, with a single light-curve shape and luminosity for a given type of SN. We then describe how the rates are calculated when the SN type has a range of luminosities and light-curve shapes — that is, with a known SN luminosity function (LF).

A1 The Control-Time Method Using a Single Light Curve

Although the method in the most basic scenario is well documented in the literature (e.g., Zwicky 1942; van den Bergh 1991; Cappellaro et al. 1993a, 1997), here we include a brief description for completeness. We follow the methodology used by Cappellaro et al. (1997) with some minor modifications.

Let $t_1, t_2, ..., t_i, ...$ be the epochs of observations, so $t_i - t_{i-1}$ is the time interval between observations $i - 1$ and i. For a possible SN in the j-th galaxy, the control time for a single image at epoch t_i, $C_{i,j}$, can be evaluated by calculating the interval of time during which the SN stays brighter than the limiting magnitude of the observation. Obviously, $C_{i,j}$ depends on the adopted peak magnitude of the SN, the light-curve shape of the SN, and the limiting magnitude of the observation.

The total control time for this j-th galaxy with a total of n observations, tC_j, can be computed as

$$tC_j = \sum_{i=1}^{n} \Delta t_i c_i, \tag{A1}$$

where

$$\Delta t_i = \begin{cases} C_{i,j} & if \ t_i - t_{i-1} \geqslant C_{i,j} \ or \ i = 1 \\ t_i - t_{i-1} & \text{otherwise,} \end{cases} \tag{A2}$$

and c_i is a correction factor introduced to account for the bias against SN discovery in the nuclear regions of galaxies in the historical rate calculations. In our study, we perform Monte Carlo simulations (§4.5) to account for the detection efficiency of each observation, rather than adopting a global correction factor.

We further define the total normalised control time as

$$t_j = tC_j L_j, \tag{A3}$$

where L_j is the galaxy luminosity (or mass). Finally, the SN rate is calculated for a galaxy sample with N_G galaxies and N_{SN} SNe as

$$\text{rate} = \frac{N_{SN}}{\sum_{j=1}^{N_G} t_j}. \tag{A4}$$

In our survey, the galaxies in the sample were observed with a relatively short time interval (§4.3), so the vast majority of control times are derived solely from the observation intervals (multiplied by the detection efficiency). Because of this, our rates have a great degree of tolerance for differences in the adopted SN light-curve shapes and LFs, especially for SNe Ia, the most luminous class. However, there are still instances where the control time needs to be derived from the limiting magnitude and the light curve, such as after a long interval of bad weather or, especially, when the galaxy under consideration reemerges into the nighttime sky.

A2 The Control-Time Method using a Known Luminosity Function

SNe display a great degree of diversity in their peak absolute luminosity and their photometric behaviours (e.g., Leibundgut et al. 1991; Filippenko 1997; Richardson et al. 2002). Even for the most homogeneous class, SNe Ia, a large fraction are either the fast-declining subluminous SN 1991bg-like objects or the slow-evolving SN 1991T-like events (Li et al. 2001). Consequently, treating a given SN type as having a single light-curve shape with a single peak absolute magnitude is an oversimplification, and has the potential to introduce large uncertainties in the final rates. In previous studies, this problem has been partly dealt with by adopting a Gaussian scatter to the peak absolute magnitudes and sometimes stretching the light curve of a SN Ia according to its luminosity (e.g., Cappellaro et al. 1997; C99; Barris et al. 2006; Neill et al. 2006; Sullivan et al. 2006 Poznanski et al. 2007; Botticella et al. 2008; Sharon et al. 2008).

As we report in Paper II, however, a Gaussian scatter is not a good approximation to the LFs of the SNe. Instead, our LFs consist of discrete peak absolute magnitudes from a complete sample of SNe, with a family of light curves for each type (component) of SN. In this section, we show

how the control time is calculated for a SN type with a known LF. Not surprisingly, the final control time is the sum of the control time for each component weighted by its relative fraction in the LF.

Let us consider a SN LF with n components and relative fractions of $f_1, f_2, ..., f_n$. We examine two scenarios. In the first scenario, a survey has complete control of every component of the SN LF during a total normalised control time of t, and a yield of N discoveries. If we use t_i as the total normalised control time and N_i as the number of SNe for the i-th component of the LF, we have the following equations:

$$\sum_{i=1}^{n} f_i = 1.0$$

$$t_i = t \qquad\qquad i = 1, 2, ... n$$

$$N_i = f_i \times N \qquad\qquad i = 1, 2, ... n \tag{A5}$$

$$\text{rate} = \sum_{i=1}^{n} \frac{N_i}{t_i} = \frac{N}{t}.$$

In the second scenario, a survey has partial control of the individual components. For the i-th component, N_i' SNe are discovered with a total normalised control time of t_i'. Under this assumption, $t_i' \leqslant t$.

Comparing the second scenario to the first, one has the following equations according to the concept of control times:

$$N_i'/t_i' = N_i/t_i = N_i/t \tag{A6}$$

This equation can be rewritten as

$$N_i' = \frac{N_i}{t} \times t_i'. \tag{A7}$$

The rate of the second scenario can be calculated as

$$
\begin{aligned}
\text{rate} &= \frac{N_1'}{t_1'} + \frac{N_2'}{t_2'} + ... + \frac{N_n'}{t_n'} \\
&= (N_1' + N_2' + ... + N_n') \times \\
&\quad [\frac{N_1'}{(N_1'+N_2'+...+N_n')} \times \frac{1}{t_1'} \\
&\quad + \frac{N_2'}{(N_1'+N_2'+...+N_n')} \times \frac{1}{t_2'} \\
&\quad + ... + \frac{N_n'}{(N_1'+N_2'+...+N_n')} \times \frac{1}{t_n'}].
\end{aligned} \tag{A8}
$$

We note that $(N_1' + N_2' + ... + N_n') = N'$ is the total number of observed SNe in the second scenario. Substituting Equation (A7) into the i-th component within the parentheses of Equation (A8) yields the following:

$$
\begin{aligned}
\frac{N_i'}{(N_1'+N_2'+...+N_n')} \times \frac{1}{t_i'} &= \frac{\frac{N_i}{t} t_i'}{\frac{N_1}{t} t_1' + \frac{N_2}{t} t_2' + ... + \frac{N_n}{t} t_n'} \times \frac{1}{t_i'} \\
&= \frac{N_i}{N_i t_1' + N_2 t_2' + ... + N_n t_n'}.
\end{aligned} \tag{A9}
$$

When Equation (A9) is substituted into Equation (A8), we have

$$
\begin{aligned}
\text{rate} &= N' \times [\frac{N_1}{N_1 t_1' + N_2 t_2' + ... + N_n t_n'} \\
&\quad + \frac{N_2}{N_1 t_1' + N_2 t_2' + ... + N_n t_n'} + ... \\
&\quad + \frac{N_n}{N_1 t_1' + N_2 t_2' + ... + N_n t_n'}] \\
&= N' \times [\frac{N_1 + N_2 + ... + N_n}{N_1 t_1' + N_2 t_2' + ... + N_n t_n'}] \\
&= N' \times [\frac{N}{N_1 t_1' + N_2 t_2' + ... + N_n t_n'}] \\
&= N' \times [\frac{1}{\frac{N_1}{N} t_1' + \frac{N_2}{N} t_2' + ... + \frac{N_n}{N} t_n'}] \\
&= \frac{N'}{\sum_{i=1}^{n} f_i t_i'} \\
&= \frac{N'}{t'},
\end{aligned} \tag{A10}
$$

where t' is the total control time for the survey. From Equation (A10), we obtain

$$t' = \sum_{i=1}^{n} f_i t_i', \tag{A11}$$

which means that the total control time is the sum of the control time of each component weighted by its fraction in the luminosity function. Equation (A11) provides the foundation on how our control time is calculated in Paper III.

Table 2. Galaxy properties in the LOSS "full" sample.[a]

field	host galaxy	$\alpha°$ (J2000)	$\delta°$	Dist[b]	src1[b]	h^c	src2[c]	$d1^d$	$d2^d$	incl.[d]	src3[d]	PA[e]	E_{BV}^f	A_i^g	B	B(err)	B0	K	K(err)
(1)	(2)	(3)	(4)	(5)	(6)	(7)	(8)	(9)	(10)	(11)	(12)	(13)	(14)	(15)	(16)	(17)	(18)	(19)	(20)
A2357+47	UGC 12889	0.00705	47.27450	71.4	LEDA	4	NED	1.87	1.18	55.4	LEDA	163.00	0.121	0.296	14.167	0.645	13.307	9.542	0.039
F00943	UGC 12890	0.02925	8.27911	159.2	NED	1	NED	1.55	0.83	62.6	LEDA	9.50	0.060	0.000	15.675	0.780	15.417	10.625	0.051
F00984	MCG -01-01-016	0.03600	-6.37397	89.0	LEDA	3	NED	1.42	0.31	87.8	LEDA	167.75	0.045	0.531	14.843	0.381	14.033	11.125	0.055
F00982	VIII Zw 494 NOTES01	0.08955	-2.61203	155.2	LEDA	1	LEDA	1.39	0.71	64.6	LEDA	127.51	0.038	0.000	15.170	0.422	14.834	10.950	0.062
UGC12893	UGC 12893	0.11760	17.21952	16.0	LEDA	7	NED	1.15	1.03	30.3	LEDA	95.00	0.034	0.089	15.383	0.390	15.141	13.452	0.223
F00473	UGC 12897	0.15810	28.38447	120.9	LEDA	3	NED	1.16	0.37	78.0	LEDA	7.20	0.062	0.543	14.822	0.075	13.925	10.369	0.040
F00472	2MASX J00004242+282	0.17670	28.36892	125.0	LEDA	2	LEDA	0.28	0.21	45.5	LEDA	94.91	0.062	0.000	17.716	0.143	17.314	12.965	0.155
F00472	CGCG 498-061	0.18345	28.40142	118.5	LEDA	6	NED	0.76	0.54	48.4	LEDA	87.30	0.062	0.135	15.661	0.119	15.150	11.367	0.066
F00472	2MASX J00004507+282	0.18780	28.37169	120.0	LEDA	2	LEDA	0.41	0.26	54.9	LEDA	158.83	0.062	0.081	17.258	0.168	16.781	13.107	0.162
F00472	UGC 12899	0.19560	28.40197	121.7	LEDA	1	NED	0.92	0.85	26.5	LEDA	—	0.062	0.000	14.636	0.128	14.235	10.176	0.051
F00998	ESO 538- G 017	0.23070	-18.95911	103.7	LEDA	6	NED	0.77	0.46	58.5	LEDA	27.22	0.021	0.352	15.569	0.349	15.071	13.004	0.139
F00460	UGC 12900	0.23355	20.33792	94.3	LEDA	6	NED	1.80	0.26	90.0	LEDA	110.00	0.078	1.413	15.611	0.329	13.823	11.151	0.061
UGC12901	UGC 12901	0.24540	28.91169	96.1	LEDA	4	NED	1.26	0.50	72.3	LEDA	44.50	0.049	0.563	14.819	0.348	13.992	10.835	0.059
F00937	NGC 7802	0.25200	6.24290	73.1	LEDA	2	NED	1.18	0.80	51.8	LEDA	54.00	0.054	0.000	14.668	0.330	14.353	9.960	0.032
F00484	UGC 12904 NOTES02	0.26520	34.65350	175.8	LEDA	3	NED	0.84	0.82	14.9	LEDA	—	0.073	0.007	15.461	0.383	14.946	11.068	0.064
F00935	IC 5374	0.26850	4.50001	122.5	LEDA	5	LEDA	0.68	0.58	35.6	LEDA	15.89	0.030	0.119	15.531	0.377	15.226	11.822	0.087
F00935	IC 5375	0.27045	4.54200	125.4	LEDA	2	NED	0.90	0.51	60.6	LEDA	177.00	0.030	0.388	15.313	0.334	14.726	11.040	0.047
F00950	KUG 2358+128A	0.30585	13.14406	75.4	LEDA	6	NED	0.75	0.30	72.5	LEDA	66.66	0.082	0.646	15.884	0.081	14.850	12.443	0.116
F00484	UGC 12904	0.30900	34.67572	179.4	LEDA	3	NED	1.02	0.69	52.3	LEDA	32.43	0.072	0.218	15.198	0.346	14.538	10.807	0.061
F00950	MCG +02-01-010	0.31290	13.11330	77.2	LEDA	7	NED	0.51	0.19	74.7	LEDA	50.00	0.081	0.725	16.773	0.202	15.663	14.140	0.264

[a] Only the first 20 entries are shown; the rest of the data are available electronically. See text for details concerning the meanings of the columns.
[b] Distance (in Mpc) and source of the distance. NED = the NASA/IPAC Extragalactic Database (http://nedwww.ipac.caltech.edu); LEDA = the HyperLeda Database (http://leda.univ-lyon1.fr).
[c] The Hubble type (with the numbering scheme in Table 1) and the source of the Hubble type.
[d] The major diameter ($d1$, in arcmin), minor diameter ($d2$, in arcmin), inclination (incl., in degrees), and the source of these data.
[e] The position angle, in degrees.
[f] The Galactic reddening $E(B-V)$, adopted from Schlegel, Finkbeiner, & Davis (1998).
[g] The internal extinction due to inclination, in magnitudes.

Table 3. Average galaxy properties in the "full" and "optimal" samples.[a]

	Full						Optimal					
Hubble	$L(B)$	$L(K)$	M	$N(B)$	$N(K)$	$N(M)$	$L(B)$	$L(K)$	M	$N(B)$	$N(K)$	$N(M)$
E	3.30(09)	19.72(49)	15.98(44)	1445	1362	1327	4.50(14)	26.61(74)	21.40(66)	750	729	724
S0	2.39(04)	13.32(22)	10.42(19)	3054	2989	2955	2.67(06)	15.26(31)	11.99(27)	1915	1881	1875
Sa	2.95(05)	11.52(20)	7.59(19)	2027	1999	1982	2.87(05)	11.56(24)	7.78(23)	1537	1513	1501
Sb	3.57(06)	11.00(19)	6.40(14)	2345	2302	2275	3.51(06)	11.52(23)	6.91(18)	1657	1618	1604
Sbc	3.53(07)	9.17(21)	4.84(13)	1735	1682	1653	3.53(08)	9.67(26)	5.25(17)	1220	1178	1162
Sc	2.96(07)	7.26(24)	3.80(22)	1587	1499	1477	2.95(08)	7.57(30)	4.08(29)	1165	1102	1093
Scd	1.69(05)	3.79(13)	1.80(08)	2101	1627	1598	1.57(05)	3.91(16)	1.94(10)	1472	1139	1120
Irr	0.93(08)	3.67(48)	2.41(40)	390	205	200	0.86(09)	3.97(58)	2.74(49)	319	161	156
$B - K$ (mag)	$L(B)$	$L(K)$	M	$N(B)$	$N(K)$	$N(M)$	$L(B)$	$L(K)$	M	$N(B)$	$N(K)$	$N(M)$
<2.3	1.99(08)	1.74(07)	0.50(02)	1703	1703	1703	1.78(09)	1.54(07)	0.44(02)	1030	1030	1030
2.3−2.8	2.81(06)	4.71(10)	1.85(04)	1779	1779	1779	2.62(07)	4.40(12)	1.73(05)	1200	1200	1200
2.8−3.1	3.48(07)	8.09(16)	3.78(07)	1774	1776	1774	3.30(07)	7.65(18)	3.57(08)	1246	1248	1246
3.1−3.4	3.47(06)	10.55(19)	5.69(10)	2015	2015	2015	3.55(08)	10.81(24)	5.83(13)	1435	1435	1435
3.4−3.7	3.21(06)	12.87(22)	8.03(14)	2144	2144	2144	3.47(07)	13.94(27)	8.71(17)	1547	1547	1547
3.7−4.0	2.98(05)	15.59(27)	11.23(20)	2147	2147	2147	3.30(07)	17.26(35)	12.43(25)	1475	1475	1475
>4.0	2.73(05)	20.86(37)	18.82(39)	1855	1855	1855	2.98(06)	23.06(48)	20.96(51)	1276	1276	1276

[a] B and K luminosities are in units of 10^{10} L$_\odot$; mass is in units of 10^{10} M$_\odot$.

Table 4. The supernova sample.[a]

SN	host galaxy	Disc. Date[b]	α°(J2000)	δ°	Offset[c]	Mag[d]	Type	Discoverer	full[e]	full-nos[e]	full-opt[e]	season[e]	season-nos[e]	season-opt[e]	LF
(1)	(2)	(3)	(4)	(5)	(6)	(7)	(8)	(9)	(10)	(11)	(12)	(13)	(14)	(15)	(16)
1998S	NGC 3877	1998-03-03	176.52574	47.48208	16.0W 46.0S	15.2	IIn	BAOSS	✓	✓					
1998cu	IC 1525	1998-06-30	359.80396	46.87550	29.2W 50.3S	18.1	II	LOSS	✓	✓	✓				
1998de	NGC 0252	1998-07-23	12.02867	27.62458	71.9E 3.4N	18.4	Ia-91bg	LOSS	✓	✓	✓	✓	✓	✓	✓
1998dh	NGC 7541	1998-07-20	348.66794	4.53725	53.5W 10.4N	16.8	Ia	LOSS	✓	✓		✓	✓		✓
1998dj	NGC 0788	1998-08-08	30.27883	-6.81800	7.1E 8.6S	16.1	Ia	LOSS	✓	✓	✓				
1998dk	UGC 00139	1998-08-19	3.63400	-0.73636	5.4E 3.1N	17.6	Ia	LOSS	✓	✓	✓	✓	✓	✓	✓
1998dl	NGC 1084	1998-08-20	41.50613	-7.57364	21.6E 11.6N	16.0	II	LOSS	✓	✓	✓				
1998dm	UGCA 017	1998-08-22	21.55821	-6.10389	13.8W 37.0S	16.8	Ia	LOSS	✓	✓		✓	✓		✓
1998dn	NGC 0337A	1998-08-19	15.36283	-7.61019	102.0W 79.0S	15.8	II	BAOSS	✓	✓	✓				
1998dt	NGC 0945	1998-09-01	37.14883	-10.54994	23.1W 39.5S	17.7	Ib	LOSS	✓	✓	✓	✓	✓	✓	✓
1998eb	NGC 1961	1998-09-17	85.55009	69.37397	38.8E 17.0S	17.8	Ia	LOSS	✓	✓	✓				
1998ec	UGC 03576	1998-09-26	103.27546	50.03947	8.7W 19.5N	16.9	Ia	BAOSS	✓	✓	✓				
1998ef	UGC 00646	1998-10-18	15.86196	32.23678	6.1E 2.1S	15.2	Ia	LOSS	✓	✓	✓	✓	✓	✓	✓
1998en	UGC 03645	1998-10-30	106.00021	50.67500	10.4W 18.3S	18.4	II	LOSS	✓	✓		✓	✓		
1998es	NGC 0632	1998-11-13	24.32292	5.88064	0.4W 10.8N	14.6	Ia-91T	LOSS	✓	✓	✓	✓	✓	✓	✓
1998fa	UGC 03513	1998-12-25	100.71462	41.42192	4.0W 3.8N	18.2	IIb	LOSS	✓	✓	✓	✓	✓	✓	
1999A	NGC 5874	1999-01-10	226.98033	54.76111	29.9E 30.1N	18.3	II	LOSS	✓	✓	✓				
1999D	IC 0694	1999-01-16	172.11826	58.56083	18.9W 4.8S	15.6	II	BAOSS	✓	✓	✓	✓	✓	✓	✓
1999aa	NGC 2595	1999-02-11	126.92512	21.48744	1.4E 31.0N	15.5	Ia-91T	Arbour	✓	✓	✓	✓	✓	✓	✓
1999ac	NGC 6063	1999-02-26	241.81255	7.97233	23.9E 29.8S	15.2	Ia-91T	LOSS	✓	✓	✓	✓	✓	✓	✓

[a]Only the first 20 entries are shown; the rest of the data are available electronically. See text for details concerning the meanings of the columns.

[b]The date of discovery.

[c]The offset (in arcsec) from the host galaxy nucleus. E = east, W = west, N = north, S = south.

[d]The magnitude at discovery.

[e]The membership in the various SN subsamples. full-nos = full-nosmall, full-opt = full-optimal, season-nos = season-nosmall, season-opt = season-optimal.